

# Face Time Traveller : Travel Through Ages Without Losing Identity

Purbayan Kar<sup>1</sup> Ayush Ghadiya<sup>1</sup> Vishal Chudasama<sup>1</sup> Pankaj Wasnik<sup>1</sup> C.V. Jawahar<sup>2</sup>  
<sup>1</sup>Sony Research India <sup>2</sup>IIT Hyderabad

{purbayan.kar, ayush.ghadiya, vishal.chudasama1, pankaj.wasnik}@sony.com, jawahar@iiit.ac.in

## Abstract

Face aging, an ill-posed problem shaped by environmental and genetic factors, is vital in entertainment, forensics, and digital archiving, where realistic age transformations must preserve both identity and visual realism. However, existing works relying on numerical age representations overlook the interplay of biological and contextual cues. Despite progress in recent face aging models, they struggle with identity preservation in wide age transformations, also static attention and optimization-heavy inversion in diffusion limit adaptability, fine-grained control and background consistency. To address these challenges, we propose Face Time Traveller (FaceTT), a diffusion-based framework that achieves high-fidelity, identity-consistent age transformation. Here, we introduce a Face-Attribute-Aware Prompt Refinement strategy that encodes intrinsic (biological) and extrinsic (environmental) aging cues for context-aware conditioning. A tuning-free Angular Inversion method is proposed that efficiently maps real faces into the diffusion latent space for fast and accurate reconstruction. Moreover, an Adaptive Attention Control mechanism is introduced that dynamically balances cross-attention for semantic aging cues and self-attention for structural and identity preservation. Extensive experiments on benchmark datasets and in-the-wild testset demonstrate that FaceTT achieves superior identity retention, background preservation and aging realism over state-of-the-art (SOTA) methods.

## 1. Introduction

Face aging, the process of simulating age progression or regression in face images, has numerous real-world applications, from digital entertainment [25, 43, 46] and medical analysis to forensic investigations [26]. As shown in Figure 1, its use extends across entertainment media, gaming, and cultural preservation. In film and advertising, productions such as *The Irishman* and public campaigns like the David Beckham malaria awareness project demonstrate the demand for realistic age transformation [46]. Traditional approaches often rely on costly and labor-intensive VFX

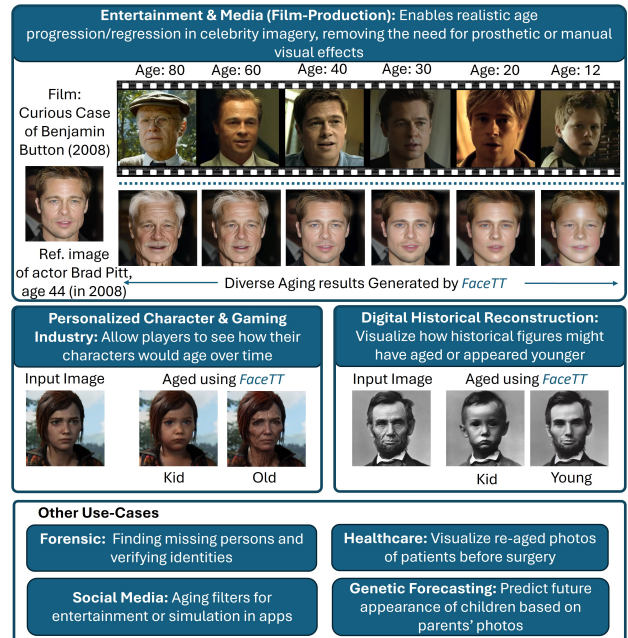


Figure 1. Illustration of real-world use cases of face aging. **Top:** The Benjamin Button example from *The Curious Case of Benjamin Button* (2008), where Brad Pitt was digitally aged using a complex hybrid VFX pipeline [8]. Modern face aging models can achieve similar visual realism at significantly lower time and cost without prosthetics or manual VFX—while preserving the actor’s identity across different lifespans. **Middle (left):** Application in personalized character and gaming environments. **Middle (right):** Digital historical reconstruction. **Bottom:** Additional use cases.

pipelines. In gaming, face aging allows characters to evolve over time, and in heritage and archival work, it supports visualizing historical figures across different life stages. Recent research advances [5, 11, 43, 46] now make high-quality face aging more accessible, reducing both time and computational cost compared to conventional workflows.

Despite promising advances, producing convincing aging results remains a complex and ill-posed problem. It requires a careful balance between altering age-relevant features and preserving age agnostic ones, such as facial identity and expression. The challenge intensifies when dealing

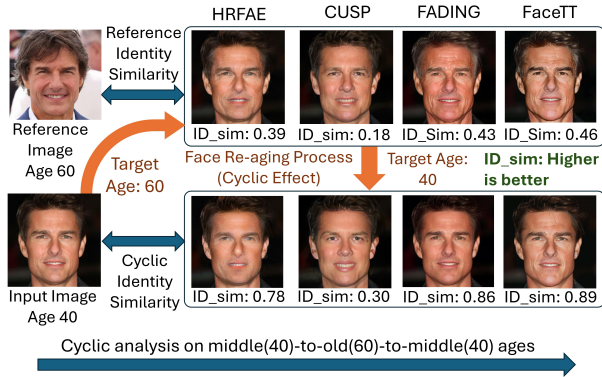


Figure 2. Illustration of cyclic identity similarity protocol. Input image (age 40) is first re-aged to the target age (60) and then reverted to its original age (40). Top row depicts the reference-based identity similarity between the re-aged and reference image, while bottom row shows the cyclic identity similarity between the input and reconstructed faces.

with significant age changes, diverse facial characteristics, and varying image conditions such as occlusions or complex backgrounds. It also involves understanding the aging process influenced by both internal factors—like genetics, hormones, and metabolism—and external ones such as UV exposure, lifestyle, and environmental effects. While intrinsic and extrinsic factors play a fundamental role in the biological aging process, this work considers their combined visual manifestations by addressing structural diversity, illumination variations, and background complexity, all while rigorously preserving the facial identity.

Recent advancements using generative adversarial networks have shown promise in addressing the face aging problem [11, 21, 29, 43, 44]. However, these methods often face difficulties in capturing high-resolution details and ensuring identity preservation. These limitations can result in artifacts or inaccurate reconstructions, which restrict their applicability to broader and more diverse scenarios. Recently, diffusion models (DMs) have emerged as a powerful alternative, offering enhanced semantic understanding and visual fidelity using inversion techniques for image synthesis and editing [2, 7, 14, 15, 18, 22, 27, 28].

While modern DMs can produce detailed results, they often fail to capture complex, abstract conditions like face aging, where intrinsic and extrinsic factors must be disentangled for realistic synthesis. To address this, we introduce *Face-Attribute-Aware Refinement* strategy that refines the prompts with identity-related and condition-driven attributes. This enables context-aware fine-tuning of DMs, leading to identity consistent, realistic face aging.

Furthermore, conventional methods [22, 28] depend on iterative optimisation to align real images with the model’s latent space, which is computationally intensive and often results in subpar reconstructions that fail to retain essential facial details. Recently, tuning-free inversion tech-

niques [14, 18, 27] have been proposed to address these issues. However, they often sacrifice reconstruction accuracy or have difficulty in generalizing across diverse image distributions. Our work advances this field by introducing a robust tuning-free *Angular Inversion* method. This approach ensures fast and high-fidelity mapping of images into the latent space, enabling efficient and precise facial edits suitable for real-time applications.

To leverage the benefits of *Angular Inversion*, it is imperative to advance attention control mechanisms for more effective guided image editing. Existing methods [4, 15, 23, 37] are typically static, applying uniform strategies across the whole image, which creates artifacts and background hallucination due to their inability to isolate and prioritize age-relevant regions. Furthermore, static approaches lack the flexibility to adapt to the semantic importance of various facial attributes, which is crucial for realistic age transformations. To address this, we introduce *Adaptive Attention Control*, a dynamic mechanism that modulates cross/self-attention during the editing process.

Existing evaluation metrics for face aging primarily rely on comparing re-aged results with real target-age images. However, such reference-based evaluations are often unreliable due to the scarcity of paired ground-truth data, making consistent identity assessment difficult. To provide a reference-independent assessment of identity consistency across diverse age transitions, we propose a new evaluation protocol termed *Cyclic Identity Similarity*, which evaluates the consistency of re-aged faces through cyclic transformations (e.g., 40→60→40), as illustrated in Figure 2.

To summarize, we propose a new face aging framework called FaceTT, where we introduce:

- **Face-Attribute-Aware Prompt Refinement** strategy that encodes intrinsic and extrinsic aging attributes to refine prompts, enabling context-aware conditioning for realistic age progression while preserving identity.
- **Angular Inversion**, a new tuning-free inversion technique that efficiently maps input images to the latent space of a pre-trained DM without iterative optimization and reduces computational overhead without sacrificing quality.
- **Adaptive Attention Control (AAC)** that determines when to apply cross-attention for semantic changes and when to use self-attention to maintain structural integrity of faces and allows precise control over aging effects while preserving identity and contextual features.
- **Cyclic Identity Similarity**, a new evaluation protocol that measures identity preservation and visual realism by assessing consistency across cyclic age transformations.

## 2. Related Works

**Inversion and Editing in DMs:** Inversion and attention control are central for faithful, structure-preserving edits in DMs. DDIM inversion [15] offers deterministic map-

ping but often introduces reconstruction errors that lead to identity drift. Null-text inversion [28] enhances stability but increases computational overhead, whereas Negative-prompt inversion [27] reduces computational overhead at the cost of image fidelity. ReNoise [10] enhances inversion robustness by mitigating error propagation. Direct inversion [18] separates source and target branches to balance content preservation and edit fidelity. Complementing these, attention-based editing frameworks such as P2P [15], PnP [37], and MasaCtrl [4] adjust attention maps to maintain spatial and semantic coherence. FPE [23] shows stable transformations, while Inversion-free editing [41] integrates cross- and self-attention control to handle both rigid and non-rigid changes effectively.

**Face Aging:** Prior face aging approaches mainly rely on conditional GANs, where age is provided as a control signal [1, 13, 40, 42, 45]. Methods like HRFAE [43] manipulate latent spaces, CUSP [11] disentangles style and content, and MyTimeMachine [30] focuses on personalized temporal aging. However, inverting real faces into GAN latent spaces often causes identity distortion [36]. While biometric constraints [3] can reduce drift, they require strong identity labels and may suppress noticeable age changes. Recently, FADING [5] introduced a diffusion-based model for age editing, but it relies on costly optimization-based inversion [28]. Multiverse Aging [12] explores condition-aware, multi-trajectory aging but trades off fine-grained reconstruction control. TimeBooth [35] improves personalization but still struggles with subtle detail, background consistency, and fine-grained identity preservation.

Despite advancements, prior works struggle to ensure high-fidelity aging, background and identity preservation under varying internal and external aging conditions. Our work addresses this gap by introducing a tuning-free *Angular Inversion*, an *Adaptive Attention Control* mechanism and a *Face-Attribute-Aware Prompt Refinement* strategy for context-aware, identity-preserved aging.

### 3. Face Aging Methodology – FaceTT

Given an image with  $\langle \text{src\_age} \rangle$ , our goal is to synthesize a new image at any target age  $\langle \text{tgt\_age} \rangle$ . Figure 3 illustrates the proposed FaceTT framework. We employ a pre-trained text-to-image diffusion model, initially fine-tuned using both age-specific prompts (*Photo of a  $\langle \text{src\_age} \rangle$  years old  $\langle \text{person} \rangle$* ) and age-agnostic prompts (*Photo of a  $\langle \text{person} \rangle$* ). To capture fine-grained cues of lifestyle and environmental aging, we incorporate the *Face-Attribute-Aware Prompt Refinement* strategy, which enriches prompts with intrinsic and extrinsic facial attributes. Building on this conditioning, the proposed *Angular Inversion* enables high-fidelity latent reconstruction, while *Adaptive Attention Control* (AAC) selectively modulates age-relevant features, ensuring precise and identity-consistent face aging.

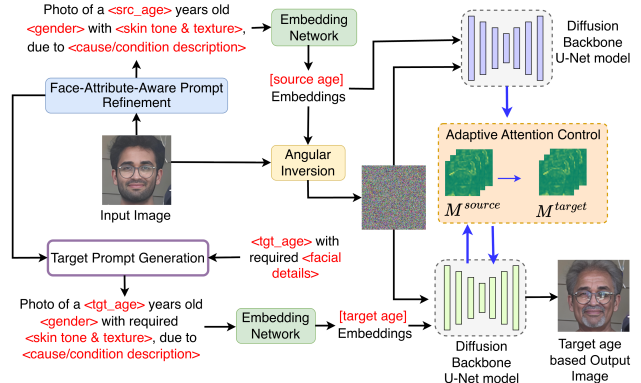


Figure 3. Overview of the proposed FaceTT framework. Given an input face, the *Face-Attribute-Aware Prompt Refinement* strategy produces a refined, attribute-rich facial prompts. These prompts are encoded using the embedding network, where the source age embeddings guide the *Angular Inversion* process to obtain high-fidelity latent reconstructions. Both source and target age embeddings are then injected into the diffusion model through *Adaptive Attention Control*, enabling precise and identity-consistent age editing. Finally, the age-transformed face is generated.

#### 3.1. Face-Attribute-Aware Prompt Refinement

While modern DMs can generate highly detailed images, they often struggle to interpret complex conditions. Fine-tuning the model with simple prompts like *Photo of a  $\langle \text{src\_age} \rangle$  years old  $\langle \text{person} \rangle$*  often fails to produce satisfactory results, as it does not explicitly describe the attributes that influence facial transformation across time. Intrinsic factors refer to internal, biological, and identity-related attributes that evolve naturally with age but are inherent to the individual — they define who the person is and how they age. In contrast, extrinsic factors capture external, lifestyle, or environmental influences that affect facial appearance but are not biologically bound — they originate from the person’s surroundings or habits.

To capture these nuances, we construct refined prompts in the form: *Photo of a  $\langle \text{src\_age} \rangle$  years old  $\langle \text{gender} \rangle$  with  $\langle \text{skin tone \& texture} \rangle$ , due to  $\langle \text{cause/condition description} \rangle$* . Here, skin tone & texture represents intrinsic factors, while cause/condition description reflects extrinsic influences. We extract age, gender, skin tone and texture, and cause/condition description from the input face using a vision language model FastVLM [38].

This refinement is crucial as high-level conditions such as “hair loss” or “weight gain” are not directly grounded in low-level visual features without sufficient contextual detail. Expanding such vague inputs into semantically rich, visually grounded descriptions enables the model to better align the generated appearance with the intended condition, thereby enhancing both realism and identity preservation.

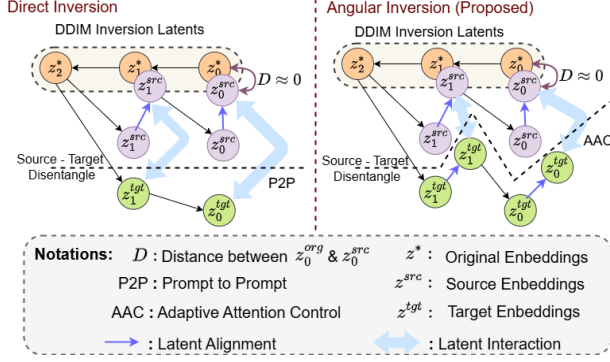


Figure 4. Illustration of the Angular Inversion technique with prior inversion techniques.

### Algorithm 1 Angular Inversion

**Require:** A face-attribute-aware source prompt embedding  $C^{src}$ , a face-attribute-aware target prompt embedding  $C^{tgt}$ , a real image or latent embedding  $z_0^{src}$ , DI: DDIM Inversion function, DF: DDIM Forward function.

**Ensure:** An edited image or latent embedding  $z_0^{tgt}$

- 1: **Part I: Inverse**  $z_0^{src}$
- 2:  $z_0^* = z_0^{src}$
- 3: **for**  $t = 1, \dots, T - 1$  **do**
- 4:  $z_t^* \leftarrow \text{DI}(z_{t-1}^*, t - 1, C^{src})$
- 5: **end for**
- 6: **Part II: Perform editing on**  $z_T^*$
- 7:  $z_T^{tgt} = z_T^*$ ;  $z_T^{src} = z_T^*$
- 8: **for**  $t = T, T - 1, \dots, 1$  **do**
- 9:  $o_{t-1}^{src} \leftarrow (z_{t-1}^* - \text{DF}_{src}(z_t^{src}, t, C^{src}))$
- 10:  $o_{t-1}^{tgt} \leftarrow (z_{t-1}^* - \text{DF}_{tgt}(z_t^{tgt}, t, C^{tgt}))$
- 11:  $\theta_{t-1}^{src} = \arccos\left(\frac{(z_{t-1}^* - z_T^*) \cdot (z_{t-1}^{src} - z_T^{src})}{\|z_{t-1}^* - z_T^*\| \|z_{t-1}^{src} - z_T^{src}\|}\right)$
- 12:  $\theta_{t-1}^{tgt} = \arccos\left(\frac{(z_{t-1}^* - z_T^*) \cdot (z_{t-1}^{tgt} - z_T^{tgt})}{\|z_{t-1}^* - z_T^*\| \|z_{t-1}^{tgt} - z_T^{tgt}\|}\right)$
- 13:  $z_{t-1}^{src} = \text{DF}_{src}(z_t^{src}, t, C^{src}) + o_{t-1}^{src}$
- 14:  $o_{t-1}^{src} \leftarrow o_{t-1}^{src} \cdot \exp(-\xi \cdot \theta_{t-1}^{src})$
- 15:  $o_{t-1}^{tgt} \leftarrow o_{t-1}^{tgt} \cdot \exp(-\xi \cdot \theta_{t-1}^{tgt})$
- 16:  $\beta_{t-1} \leftarrow \text{cosine\_similarity}(z_{t-1}^*, z_{t-1}^{tgt})$
- 17:  $z_{t-1}^{tgt} \leftarrow \text{DF}_{tgt}(z_t^{tgt}, t, C^{tgt}) + \beta_{t-1} \cdot o_{t-1}^{tgt} + (1 - \beta_{t-1}) \cdot o_{t-1}^{src}$
- 18: **end for**
- 19: **return**  $z_0^{tgt}$

## 3.2. Angular Inversion Technique

**Background & Preliminaries:** DMs iteratively transform noise  $z_T$  into an image  $z_0$  through Gaussian perturbations  $\epsilon \sim \mathcal{N}(0, 1)$ , with  $z_t = \sqrt{\alpha_t} z_0 + \sqrt{1 - \alpha_t} \epsilon$ . A denoiser  $\epsilon_\theta$  is trained to predict  $\epsilon(z_t, t)$ . DDIM sampling [34] generates  $z_{t-1}$  via the learned noise estimate. DDIM inversion reverses this process as  $z_t^* = \frac{\sqrt{\alpha_t}}{\sqrt{\alpha_{t-1}}} z_{t-1}^* + \sqrt{\alpha_t} \left( \sqrt{\frac{1}{\alpha_t} - 1} - \sqrt{\frac{1}{\alpha_{t-1}} - 1} \right) \epsilon_\theta(z_{t-1}^*, t - 1)$ , though it often yields imperfect reconstruction. CFG [16] blends conditional and unconditional denoising,  $\epsilon_\theta(z_t, t, C, \emptyset) = w \epsilon_\theta(z_t, t, C) + (1 - w) \epsilon_\theta(z_t, t, \emptyset)$ , enhancing prompt ( $C$ ) adherence but introducing latent inconsistencies between

original and edited image’s latent trajectories  $z_t^{src}$  and  $z_t^{tgt}$ .

To mitigate inconsistencies from DDIM inversion and CFG, optimization-based methods [14, 17, 18, 27, 28] have been proposed. Null-Text Inversion [28] refines a null-text embedding to minimize  $z_t^{src/tgt} - z_t^*$ , but is slow and prone to latent misalignment. Direct Inversion [18] improves content preservation and edit fidelity by decoupling source and target branches, yet struggles with complex, non-linear edits and may underperform when substantial semantic changes (wide age transformations) are required.

To address the limitations of existing inversion techniques, we propose *Angular Inversion*, which disentangles the source and target branches. This separation allows each branch to be optimized independently (see Figure 4). In the source branch, we directly add  $(z_t^* - z_t^{src})$  to  $z_t^{src}$ . In the target branch, rather than leaving it unaltered, we scale  $(z_t^* - z_t^{src})$  by  $\exp(-\xi \cdot \angle z_t^* z_T^{src})$  and  $(z_t^* - z_t^{tgt})$  by  $\exp(-\xi \cdot \angle z_t^* z_T^{tgt})$ , where  $\xi$  is a hyper-parameter.

During iteration, large angles indicate misalignment. To mitigate this, we downweight updates proportionally, enabling gradual adjustments and preventing disruptive shifts in latent representations. This stabilizes the target branch and avoids errors during stepwise generation.

Next, a linear combination of the scaled  $(z_t^* - z_t^{src})$  and  $(z_t^* - z_t^{tgt})$ , weighted by the cosine similarity between  $z_t^*$  and  $z_t^{tgt}$ , is added back to  $z_t^{tgt}$ . High similarity shifts focus toward  $(z_t^* - z_t^{tgt})$  to improve edit fidelity, while low similarity increases the influence of  $(z_t^* - z_t^{src})$ .

This method enables efficient, high-quality edits by (1) removing costly optimization, (2) reducing discrepancies between source and target latent spaces, (3) improving target edit fidelity through better alignment, and (4) preserving the diffusion model’s input distribution. A detailed description is provided in Algorithm 1.

## 3.3. Adaptive Attention Control

We investigate the distinct roles of cross- and self-attention in face aging using Stable Diffusion to understand their impact on identity-consistent age transformation (see supplementary-S1). Our analysis shows that cross-attention primarily captures semantic age-related cues—such as wrinkles, skin tone, and hair color—driven by the conditioning text. In contrast self-attention preserves facial geometry, expression, and identity coherence. This probing study enables fine-grained manipulation of facial features by selectively modifying cross-attention maps, allowing controlled semantic aging while retaining the original face layout. However, applying cross-attention control throughout the full sampling process tends to over-constrain spatial alignment, limiting the model’s flexibility to generate realistic age variations. Hence, following [15], we restrict cross-attention control to the early denoising steps (before  $\tau_1$ ), ensuring a balanced trade-off between semantic

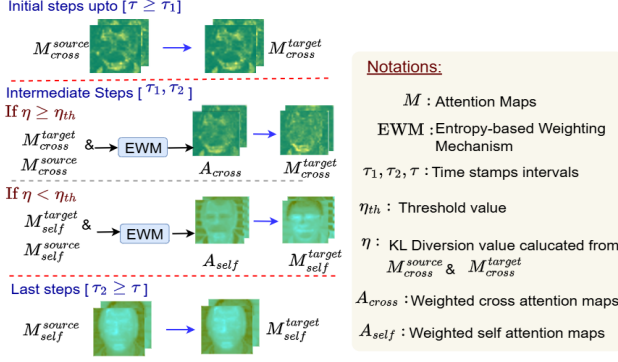


Figure 5. Illustration of Adaptive Attention Control Mechanism.

### Algorithm 2 Adaptive Attention Control

**Require:** Face-attribute-aware source prompt embedding  $C^{src}$ , face-attribute-aware target prompt embedding  $C^{tgt}$ , real image or latent embedding  $z_0^{src}$ ,  $H$ : entropy function,  $DI$ : DDIM Inversion function,  $DF$ : DDIM Forward function.

**Ensure:** An edited image or latent embedding  $z_0^{tgt}$

```

1: Part I: Inverse  $z_0^{src}$ 
2:  $z_0^* = z_0^{src}$ 
3: for  $t = 1, \dots, T - 1$  do
4:    $z_t^* \leftarrow DI(z_{t-1}^*, t - 1, C^{src})$ 
5: end for
6: Part II: Perform editing on  $z_T^*$ 
7:  $z_T^{tgt} = z_T^*$ ;  $z_T^{src} = z_T^*$ 
8: for  $t = T, T - 1, \dots, 1$  do
9:    $z_{t-1}^{src}, M_{self}^{src}, M_{cross}^{src} \leftarrow DF_{src}(z_t^{src}, t, C^{src})$ 
10:   $M_{self}^{tgt}, M_{cross}^{tgt} \leftarrow DF_{tgt}(z_t^{tgt}, t, C^{tgt})$ 
11:  if  $t > \tau_1$  then
12:     $z_{t-1}^{tgt} \leftarrow DF_{tgt}(z_t^{tgt}, t, C^{tgt}) \{M_{cross}^{tgt} \leftarrow M_{cross}^{src}\}$ 
13:  else if  $\tau_2 \leq t \leq \tau_1$  then
14:     $\eta \leftarrow D_{KL}(M_{cross}^{src} || M_{cross}^{tgt})$ 
15:    if  $\eta > \eta_{th}$  then
16:       $w_{t-1} \leftarrow 1 - H(M_{cross}^{src})$ 
17:       $A_{cross} \leftarrow w_{t-1} \cdot M_{cross}^{src} + (1 - w_{t-1}) \cdot M_{cross}^{tgt}$ 
18:       $z_{t-1}^{tgt} \leftarrow DF_{tgt}(z_t^{tgt}, t, C^{tgt}) \{M_{cross}^{tgt} \leftarrow A_{cross}\}$ 
19:    else
20:       $w_{t-1} \leftarrow 1 - H(M_{self}^{src})$ 
21:       $A_{self} \leftarrow w_{t-1} \cdot M_{self}^{src} + (1 - w_{t-1}) \cdot M_{self}^{tgt}$ 
22:       $z_{t-1}^{tgt} \leftarrow DF_{tgt}(z_t^{tgt}, t, C^{tgt}) \{M_{self}^{tgt} \leftarrow A_{self}\}$ 
23:    end if
24:  else
25:     $z_{t-1}^{tgt} \leftarrow DF_{tgt}(z_t^{tgt}, t, C^{tgt}) \{M_{self}^{tgt} \leftarrow M_{self}^{src}\}$ 
26:  end if
27: end for
28: return  $z_0^{tgt}$ 

```

transformation and structural preservation.

A key limitation of cross-attention control in face aging is its inability to capture non-rigid facial deformations that naturally occur with aging. As observed in [4, 23], such flexible spatial adaptations are better handled by self-attention, where query maps preserve facial layout while accommodating age-related semantic variations. Our probing analysis (see supplementary-S1) confirms this behavior. Following [23], we replace the self-attention maps of layers 4–14 in the target image with those from the

source, but only after  $\tau_2$  steps. This design enables non-rigid yet identity-consistent transformations without introducing distortions—particularly around accessories (e.g., glasses, hats, earrings) and in complex background regions.

During the intermediate denoising phase ( $\tau_1 - \tau_2$ ), achieving a balance between rigid and non-rigid semantic changes is challenging. As noted in [41], naive fusion of cross- and self-attention often leads to sub-optimal edits in dual-branch frameworks. To address this, we dynamically regulate the attention control parameter  $\eta$  based on the KL-divergence between the source and target cross-attention maps ( $M_{cross}^{src}$  and  $M_{cross}^{tgt}$ ). When  $\eta$  is below a defined threshold ( $\eta_{th}$ ), self-attention dominates to preserve fine structural details—such as the eyes, nose, and jawline—ensuring identity stability. Conversely, when  $\eta > \eta_{th}$ , the model prioritizes cross-attention to introduce more pronounced semantic transformations, such as deep wrinkles or other age-specific facial modifications.

Instead of directly replacing target attention maps with those of the source, the intermediate stage blends them to ensure a smooth transition and prevent abrupt changes. The blending weight is defined as  $w_t \leftarrow 1 - H(M_{cross}^{src/tgt})$ , which determines the relative influence of the source (either self- or cross-attention) and target attention maps. Here,  $H(\cdot)$  denotes the entropy of the source attention map, reflecting how focused or dispersed the attention distribution is. Low entropy (i.e., concentrated attention) yields  $w_t \approx 1$ , emphasizing key structural elements of the source image to preserve identity. Conversely, high entropy produces  $w_t \approx 0$ , allowing greater flexibility for integrating target-specific attributes and enabling non-rigid, age-related transformations. A similar weighting scheme is applied to self-attention maps. The full procedure is outlined in Algorithm 2 and visualized in Figure 5.

## 4. Experimental Analysis

**Implementation details:** We leverage the pre-trained Stable Diffusion model [32] and finetune it on the FFHQ-Aging dataset [44] for 150 steps with a batch size of 2. We incorporate the central age of the true age group into the finetuning prompt as  $\langle src\_age \rangle$ . We employ Adam optimizer with a learning rate of  $5 \times 10^{-6}$ . For inversion, we set  $\xi$  to 1.2. During attention control,  $\eta_{th}$  is fixed at 0.05, while  $\tau_1$  and  $\tau_2$  are set to 35 and 15, respectively. All experiments are conducted on a single A100 GPU. We compare our model against SOTA face aging methods, including HRFAE [43], CUSP [11] and FADING [5], with results reproduced using their official repos for fair comparison.

**Dataset details:** We use two benchmark datasets, CelebA-HQ [19] and FFHQ-Aging [44], along with an in-the-wild celebrity age progression test set. CelebA-HQ is used only for evaluation. Following prior works [43, 45], age labels are obtained using the DEX classifier [33]. We sample

1,000 “young” images and age them to 60, with all images resized to  $512 \times 512$ . FFHQ-Aging consists of 70,000 images at  $1024 \times 1024$  resolution, grouped into ten age ranges from 0–2 to 70+ years. For the in-the-wild evaluation, we construct a celebrity age progression test set by curating five celebrities with publicly available, license-compliant images across three age ranges:  $\{20-40\}$ ,  $\{40-60\}$  and  $\{60-80\}$  years. One representative image per range yields a total of 15 images, enabling both reference-based and cyclic evaluations of aging quality and identity consistency.

**Cyclic Identity Similarity Protocol:** Traditional evaluations rely on comparing re-aged images with real target-age references. However, such reference-based comparisons are often unreliable due to limited ground-truth availability and high inter-age variations in real datasets. To address this limitation, we propose *Cyclic Identity Similarity*, a new evaluation protocol that eliminates dependence on external ground-truth images. It consists of two analysis: *Cyclic Identity Similarity* and *Reference-Based Identity Similarity*.

- Cyclic Identity Similarity ( $ID_{sim}^{cyc}$ ):** Given an input image  $I_{20-40}$  from the celebrity testset, we first age it to a target age range, producing  $I'_{40-60}$ , and then revert the process to reconstruct  $I''_{20-40}$ . Identity preservation across this round-trip transformation is measured as  $ID_{sim}^{cyc}(I_{20-40}) = \text{sim}(f(I_{20-40}), f(I''_{20-40}))$ , where  $f(\cdot)$  is a pretrained ArcFace [9] model. This assesses identity consistency over cyclic aging paths ( $\{20-40\} \rightarrow \{40-60\} \rightarrow \{20-40\}$ ).
- Reference-Based Identity Similarity ( $ID_{sim}^{ref}$ ):** Following [30], in the case of celebrity testset, for each re-aged image  $I'_a$  (where  $a \in \{\{40-60\}, \{60-80\}\}$ ), we compare it to the corresponding real image  $I_a$  of the same individual in the target age group:  $ID_{sim}^{ref}(I_a) = \text{sim}(f(I_a), f(I'_a))$ . This evaluates how closely the synthesized aged face matches the true target-age identity.

The averaged  $ID_{sim}^{cyc}$  and  $ID_{sim}^{ref}$  across all subjects serve as our primary quantitative measures.

**Additional Evaluation Metrics:** Following [5], we evaluate the face aging methods on 1) Mean Absolute Error (MAE), which compares the predictions of an age estimator to the target age; (2) Gender, Smile and Facial Expression Preservation, which measures the retention percentage of these attributes after transformation; (3) Blurriness, which assesses the degree of a facial blur; (4) Kernel-Inception Distance (KID), which quantifies the distance between real and generated images within the corresponding age groups. We employ Face++<sup>1</sup> to measure aging accuracy, attribute preservation and blurriness.

#### 4.1. Comparison with SOTA methods

**Face Aging methods:** Table 1 presents a comparison on CelebA-HQ dataset. Note that a 5.14-year discrepancy (i.e.,

<sup>1</sup>faceplusplus.com/

Table 1. Quantitative results on CelebA-HQ dataset on the young-to-60 task. Best score: in red, second-best score: in green.

Method	Predicted age	Blur ↓	Gender ↑	Smiling ↑	Neutral ↑	Happy ↑
Real images	65.14 ± 4.86	1.73	—	—	—	—
HRFAE	55.05 ± 9.18	3.42	94.80	74.60	61.15	71.09
CUSP	57.57 ± 7.88	3.39	89.79	75.88	60.67	70.87
FADING	69.88 ± 6.20	2.18	98.44	76.17	56.54	73.19
FaceTT	62.05 ± 6.81	2.18	99.79	78.31	62.67	72.17

Table 2. Quantitative results on different age groups of FFHQ-Aging dataset. Best score: in red, second-best score: in green.

Method	0-2	3-6	7-9	10-14	15-19	20-29	30-39	40-49	50-69	70+	Mean
Mean Absolute Error - MAE (lower is better)											
HRFAE	35.43	32.49	36.43	25.95	21.35	7.43	8.75	13.72	15.75	21.13	21.84
CUSP	19.39	23.96	21.96	14.21	9.81	13.11	14.09	15.86	16.09	15.56	16.40
FADING	11.63	16.97	18.76	13.70	7.03	11.18	13.98	15.45	14.15	11.91	13.47
FaceTT	11.05	16.24	12.45	12.31	7.10	8.92	11.23	12.31	11.12	11.35	11.40
Gender Accuracy (higher is better)											
HRFAE	0.48	0.52	0.41	0.42	0.28	0.40	0.50	0.42	0.52	0.55	0.45
CUSP	0.47	0.56	0.60	0.58	0.50	0.51	0.43	0.45	0.49	0.53	0.51
FADING	0.51	0.61	0.57	0.53	0.53	0.52	0.40	0.47	0.52	0.55	0.57
FaceTT	0.55	0.63	0.61	0.65	0.71	0.59	0.45	0.65	0.71	0.63	0.62
Kernel Inception Distance - KID (lower is better)											
HRFAE	0.37	0.36	0.34	0.49	0.37	0.31	0.19	0.35	0.40	0.60	0.34
CUSP	13.10	7.20	3.70	1.60	0.70	0.41	0.34	0.31	0.53	2.70	3.06
FADING	10.32	4.50	2.20	1.09	0.40	0.35	0.40	0.28	0.60	1.60	2.03
FaceTT	12.18	1.03	0.76	0.39	0.36	0.30	0.18	0.30	0.17	0.20	1.58

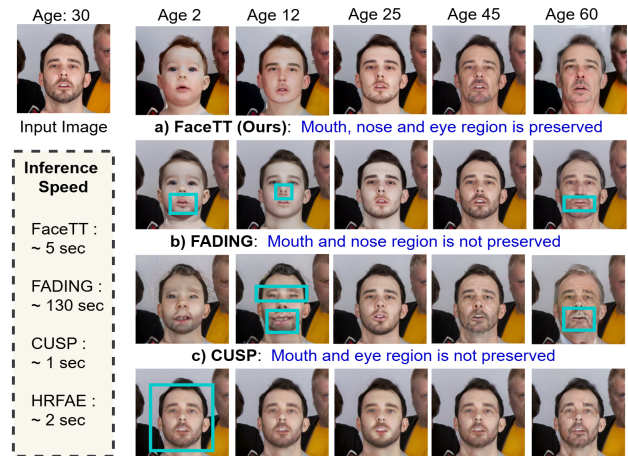


Figure 6. Visual comparison with SOTA face aging methods.

65.14; first row) is reported for our training subset (age label 60) between the DEX classifier used for inference and the Face++ classifier used for evaluation. The results of the proposed FaceTT model are closer to the target age of 60. Additionally, it obtains highest score in gender preservation, demonstrating its effectiveness in maintaining age-independent characteristics.

Table 2 depicts a comparison of the FFHQ-Aging dataset where the proposed FaceTT achieves a better MAE score, indicating improved aging accuracy, with a 15% improvement over FADING. Furthermore, the proposed method obtains better gender accuracy across all age brackets, highlighting its ability to preserve essential identity attributes as age progresses. The KID analysis further supports our results. The HRFAE exhibits minimal changes across ages (see Figure 6), resulting in a low KID score.

Figure 6 qualitatively validates that the proposed FaceTT achieves better visual fidelity with minimal artifacts. It gen-

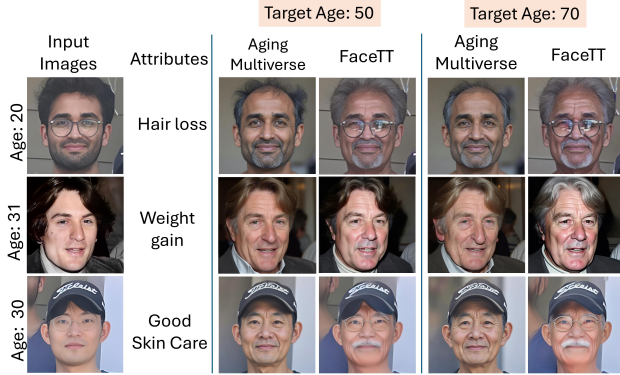


Figure 7. Visual comparison with Aging Multiverse [12]. Our method generates better attribute-aware aging while preserving background details (see rows 1 & 2), skin tone (see rows 2 & 3) and accessories such as eyeglasses (see rows 1 & 3).

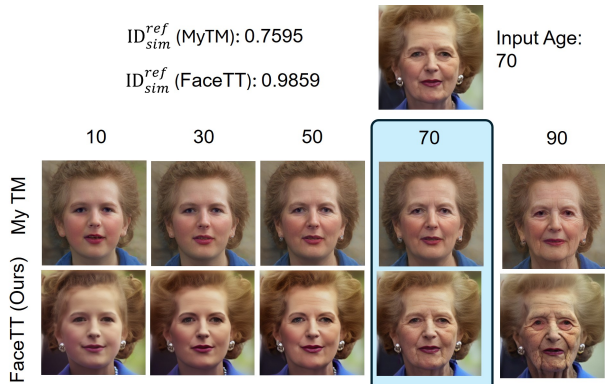


Figure 8. Visual comparison with MyTM [30]. MyTM fails to preserve the background (missing dark shadow in the lower-left region) and misses the accessory (earrings). FaceTT maintains consistent background and accessory details.

erates an image in 5 seconds, while FADING takes around 130 seconds. This demonstrates that our framework enhances reconstruction quality with a significant reduced inference time. A detailed analysis with more examples is provided in supplementary-S2.

**Comparison with Recent Unpublished Works:** Additionally, we include visual comparisons with two recent unpublished works—Aging Multiverse<sup>2</sup> [12] and MyTimeMachine (MyTM)<sup>3</sup> [30]—using the results available on their official webpages. As shown in Figure 7, our method produces more realistic attribute-aware age progression than Aging Multiverse, while preserving skin tone, background details, and accessories (e.g., eyeglasses). When compared to MyTM (Figure 8), which emphasizes personalized temporal aging, our method achieves natural and accurate aging transformations, particularly at older ages, while also effectively preserving background details and object consistency such as earrings. These findings are consistent with our im-

<sup>2</sup>agingmultiverse.github.io/

<sup>3</sup>mytimemachine.github.io/

Table 3. Comparison of  $ID_{sim}$  scores across different methods.

$ID_{sim}$	HRAE	CUSP	FADING	FaceTT
$ID_{sim}^{cyc}$ in FFHQ test-set	0.61	0.55	0.67	0.69
$ID_{sim}^{cyc}$ in Celebrity Test-set	0.60	0.39	0.77	0.80
$ID_{sim}^{ref}$ in Celebrity Test-set	0.42	0.32	0.50	0.55

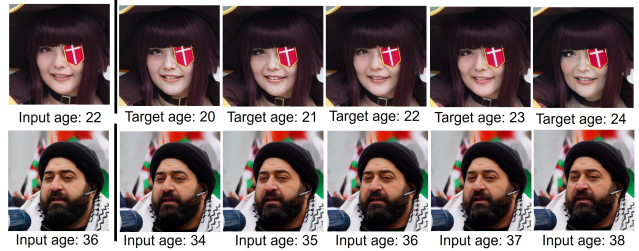


Figure 9. Short-Range Aging analysis: FaceTT maintains strong identity consistency across closely spaced age targets.

Table 4. Biometric matching results between original and re-aged images on FFHQ dataset. The metrics are False Non Match Rate (FNMR) at False Match Rate (FMR) = 0.01/0.1%. Lower is better.

Method	2	12	25	35	45	60
CUSP	0.52/0.28	0.22/0.11	0.31/0.13	0.27/0.09	0.23/0.07	0.45/0.10
FADING	0.55/0.49	0.11/0.07	0.26/0.09	0.25/0.07	0.25/0.07	0.33/0.12
FaceTT	0.60/0.49	0.18/0.10	0.06/0.06	0.02/0.01	0.03/0.02	0.13/0.07

Table 5. Impact of proposed components on CelebA-HQ for young-to-60 task.

Angular Inversion	AAC	Predicted Age	Blur ↓	Gender ↑	Smiling ↑	Neutral ↑	Happy ↑
Real Images		65.14 ± 4.86	1.73	—	—	—	—
×	×	69.88 ± 6.20	2.18	98.44	76.17	56.54	73.19
×	✓	61.70 ± 6.30	2.21	99.22	73.78	64.99	66.72
✓	×	61.25 ± 6.20	2.89	99.02	68.58	61.37	64.48
✓	✓	62.05 ± 6.81	2.18	99.79	78.31	62.67	72.17

proved  $ID_{sim}^{ref}$  scores, highlighting superior identity preservation.

## 4.2. Evaluation on Identity Preservation

**Cyclic / Reference based Aging Analysis:** Table 3 reports the  $ID_{sim}$  scores for face aging methods on both the FFHQ test set and the celebrity age progression test set. For the FFHQ dataset, we divide samples into *young* (<40) and *old* (>40) groups. Faces in the young group are aged to 60 and then reverted back to compute the  $ID_{sim}^{cyc}$ , while faces in the old group are de-aged to 20 and then restored to compute the same measure. This bidirectional procedure provides a balanced evaluation of both aging and de-aging identity consistency. For the celebrity test set, we report both  $ID_{sim}^{cyc}$  and  $ID_{sim}^{ref}$ . The cyclic score is computed by averaging  $ID_{sim}^{cyc}$  across all possible age-range cycles. The  $ID_{sim}^{ref}$  compares each re-aged image to the corresponding real target-age image. Across both datasets, the proposed FaceTT consistently achieves the highest  $ID_{sim}^{cyc}$  and  $ID_{sim}^{ref}$  scores, indicating superior identity preservation and more stable bidirectional age transformations compared to others.

**Short-Range Aging Analysis:** We further conduct a qualitative analysis to assess identity retention under fine-grained age changes. Figure S7 shows examples where each face is re-aged within a narrow range around the original age (e.g.,

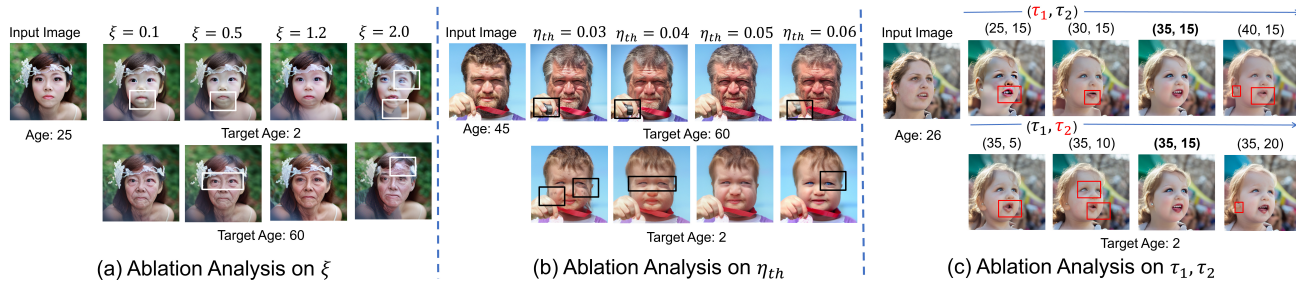


Figure 10. Ablation analysis on hyper-parameters (a)  $\xi$ ; (b)  $\eta_{th}$ ; (c)  $\tau_1, \tau_2$ . (More examples are provided in supplementary-S3).

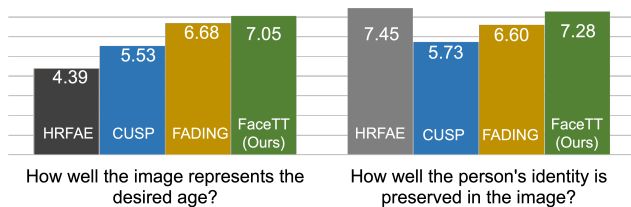


Figure 11. User study Analysis: our method consistently scores high in both aging and identity preservation. HRFAE’s high score for identity preservation stems from its limited aging ability, often producing results nearly identical to the input.

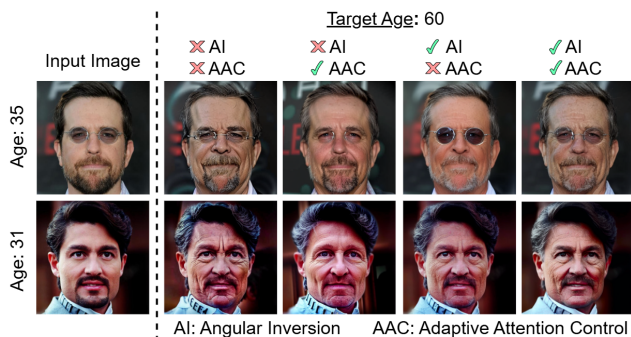


Figure 12. Ablation analysis on CelebA-HQ for young-to-60 task.

$x - 2 \leq \text{target age} \leq x + 2$ ). Our model produces visually consistent faces across these small age shifts, indicating strong identity stability.

**Biometric Matching Analysis:** Inspired by [3], we perform a biometric verification study on the FFHQ dataset. Following the standard verification protocol, we report the *False Non-Match Rate (FNMR)* at two operating points of *False Match Rate (FMR)* = 0.01 and 0.1%. This experiment measures how well aged faces remain recognizable to a pretrained face recognition model [9]. Table 4 presents FNMR@FMR across six aging distances (2, 12, 25, 35, 45, and 60 years) for CUSP, FADING, and our FaceTT. Lower FNMR indicates stronger identity retention. FaceTT consistently achieves the lowest FNMR (particularly for the middle and older age groups). Notably, at a 35-year aging distance, FaceTT achieves an FNMR of 0.02/0.01, representing a significant improvement over competing methods.

**User Study Analysis:** We conducted a user study with 35 participants on 14 images (10 from FFHQ and 4 in-the-wild) re-aged to six target ages (2, 12, 25, 35, 45 and 60).

Participants rated each result (1–10) for age accuracy and identity preservation. As shown in Figure 11, our method ranks highest in achieving the target age and second-highest in identity preservation. HRFAE scores high in identity preservation mainly because it performs minimal aging and often produces images nearly identical (Figure 6).

### 4.3. Ablation Analysis

**Impact of individual components:** To validate the impact of our proposed *Angular Inversion* and *AAC* modules, we conducted ablation studies on the CelebA-HQ dataset. The results, presented in Table 5 and Figure 12 demonstrate that both the *Angular Inversion* and *AAC* modules contribute to improving the overall performance.

**Sensitivity Analysis of Hyper-parameters:** Figure 10 presents the ablation analysis of  $\xi$ ,  $\eta_{th}$ ,  $\tau_1$ , and  $\tau_2$ .

- In Figure 10(a), low  $\xi$  (0.1, 0.5) yields minimal change—identity is preserved but aging is weak—while high  $\xi$  (2.0) causes excessive edits and identity loss. The optimal balance is achieved at  $\xi = 1.2$ .
- Figure 10(b) shows that a low  $\eta_{th}$  (0.03) over-preserved source traits, limiting aging, whereas a high value (0.06) over-modifies details and introduces artifacts.  $\eta_{th} = 0.05$  produces the most natural aging with consistent identity.
- In Figure 10(c), low  $\tau_1$  (25) retains too many source attributes, while high values (40) cause exaggerated changes.  $\tau_2$  similarly controls transformation smoothness. The optimal configuration  $(\tau_1, \tau_2) = (35, 15)$  yields realistic aging with strong structural consistency.

## 5. Conclusion

In this paper, we present FaceTT, a novel diffusion-based framework for realistic and identity-consistent face aging, enabled by Face-Attribute-Aware Prompt Refinement, Angular Inversion, and Adaptive Attention Control. Our experiments demonstrate strong aging realism, background preservation, and superior identity retention compared to existing methods. In future work, we plan to extend FaceTT to support temporal age progression in videos, incorporating motion and expression consistency across frames, thereby broadening its applicability to real-world scenarios.

## References

- [1] Grigory Antipov, Moez Baccouche, and Jean-Luc Dugelay. Face aging with conditional generative adversarial networks. In *2017 IEEE international conference on image processing (ICIP)*, pages 2089–2093. IEEE, 2017. 3
- [2] Omri Avrahami, Ohad Fried, and Dani Lischinski. Blended latent diffusion. *ACM transactions on graphics (TOG)*, 42(4):1–11, 2023. 2
- [3] Sudipta Banerjee, Govind Mittal, Ameya Joshi, Chinmay Hegde, and Nasir Memon. Identity-preserving aging of face images via latent diffusion models. In *2023 IEEE International Joint Conference on Biometrics (IJCB)*, pages 1–10. IEEE, 2023. 3, 8
- [4] Mingdeng Cao, Xintao Wang, Zhongang Qi, Ying Shan, Xiaohu Qie, and Yinqiang Zheng. Masactrl: Tuning-free mutual self-attention control for consistent image synthesis and editing. In *Proceedings of the IEEE/CVF International Conference on Computer Vision*, pages 22560–22570, 2023. 2, 3, 5, 9, 12
- [5] Xiangyi Chen and Stéphane Lathuilière. Face aging via diffusion-based editing. In *BMVC*, 2023. 1, 3, 5, 6, 9
- [6] Kevin Clark, Urvashi Khandelwal, Omer Levy, and Christopher D Manning. What does bert look at? an analysis of bert’s attention. *arXiv preprint arXiv:1906.04341*, 2019. 2
- [7] Guillaume Couairon, Jakob Verbeek, Holger Schwenk, and Matthieu Cord. Diffedit: Diffusion-based semantic image editing with mask guidance. In *ICLR 2023 (Eleventh International Conference on Learning Representations)*, 2023. 2
- [8] Adrian Danks. Not dark yet: Life reversed in ‘the curious case of benjamin button’. *Screen Education*, (97):94–100, 2020. 1
- [9] Jiankang Deng, Jia Guo, Niannan Xue, and Stefanos Zafeiriou. Arcface: Additive angular margin loss for deep face recognition. In *Proceedings of the IEEE/CVF conference on computer vision and pattern recognition*, pages 4690–4699, 2019. 6, 8
- [10] Daniel Garibi, Or Patashnik, Andrey Voynov, Hadar Averbuch-Elor, and Daniel Cohen-Or. Renoise: Real image inversion through iterative noising. In *European Conference on Computer Vision*, pages 395–413. Springer, 2024. 3
- [11] Guillermo Gomez-Trenado, Stéphane Lathuilière, Pablo Mesejo, and Óscar Cordón. Custom structure preservation in face aging. In *European Conference on Computer Vision*, pages 565–580. Springer, 2022. 1, 2, 3, 5, 9
- [12] Bang Gong, Luchao Qi, Jiaye Wu, Zhicheng Fu, Chunbo Song, David W Jacobs, John Nicholson, and Roni Sengupta. The aging multiverse: Generating condition-aware facial aging tree via training-free diffusion. *arXiv preprint arXiv:2506.21008*, 2025. 3, 7
- [13] Xiangyu Gong, Weixin Li, Amanda W L Yao, and Ling Shao. Wasserstein divergence gan with cross-age identity expert and attribute retainer for facial age transformation. *IEEE Transactions on Neural Networks and Learning Systems*, 31(6):1941–1956, 2019. 3
- [14] Ligong Han, Song Wen, Qi Chen, Zhixing Zhang, Kunpeng Song, Mengwei Ren, Ruijiang Gao, Anastasis Stathopoulos, Xiaoxiao He, Yuxiao Chen, et al. Proxedit: Improving tuning-free real image editing with proximal guidance. In *Proceedings of the IEEE/CVF Winter Conference on Applications of Computer Vision*, pages 4291–4301, 2024. 2, 4, 8, 9
- [15] Amir Hertz, Ron Mokady, Jay Tenenbaum, Kfir Aberman, Yael Pritch, and Daniel Cohen-Or. Prompt-to-prompt image editing with cross-attention control. In *ICLR*, 2023. 2, 3, 4, 9, 12
- [16] Jonathan Ho and Tim Salimans. Classifier-free diffusion guidance. *arXiv preprint arXiv:2207.12598*, 2022. 4
- [17] Inbar Huberman-Spiegelglas, Vladimir Kulikov, and Tomer Michaeli. An edit friendly ddpn noise space: Inversion and manipulations. In *Proceedings of the IEEE/CVF Conference on Computer Vision and Pattern Recognition*, pages 12469–12478, 2024. 4
- [18] Xuan Ju, Ailing Zeng, Yuxuan Bian, Shaoteng Liu, and Qiang Xu. Pnp inversion: Boosting diffusion-based editing with 3 lines of code. *International Conference on Learning Representations (ICLR)*, 2024. 2, 3, 4, 8, 9
- [19] Tero Karras, Samuli Laine, and Timo Aila. A style-based generator architecture for generative adversarial networks. In *Proceedings of the IEEE/CVF conference on computer vision and pattern recognition*, pages 4401–4410, 2019. 5
- [20] Jacob Devlin Ming-Wei Chang Kenton and Lee Kristina Toutanova. Bert: Pre-training of deep bidirectional transformers for language understanding. In *Proceedings of naacl-HLT*, page 2. Minneapolis, Minnesota, 2019. 3
- [21] Linsen Li, Wenhan Liu, Juefei-Xu Jiang, Sheng Wang, Xuan Liu, Xiang Wu, and Nenghai Yu. Re-aging gan: Toward personalized face age transformation. In *Proceedings of the IEEE/CVF Conference on Computer Vision and Pattern Recognition (CVPR) Workshops*, pages 818–819, 2020. 2
- [22] Senmao Li, Joost van de Weijer, Taihang Hu, Fahad Shahbaz Khan, Qibin Hou, Yaxing Wang, and Jian Yang. Stylediffusion: Prompt-embedding inversion for text-based editing. *arXiv preprint arXiv:2303.15649*, 2023. 2
- [23] Bingyan Liu, Chengyu Wang, Tingfeng Cao, Kui Jia, and Jun Huang. Towards understanding cross and self-attention in stable diffusion for text-guided image editing. In *Proceedings of the IEEE/CVF Conference on Computer Vision and Pattern Recognition*, pages 7817–7826, 2024. 2, 3, 5, 9, 12
- [24] Nelson F Liu, Matt Gardner, Yonatan Belinkov, Matthew E Peters, and Noah A Smith. Linguistic knowledge and transferability of contextual representations. In *Proceedings of NAACL-HLT*, pages 1073–1094, 2019. 2
- [25] Kathleen Looch. On the realist aesthetics of digital de-aging in contemporary hollywood cinema. *Orbis Litterarum*, 76(4):214–225, 2021. 1
- [26] Jason Elroy Martis, MS Sannidhan, N Pratheeksha Hegde, and L Sadananda. Precision sketching with de-aging networks in forensics. *Frontiers in Signal Processing*, 4: 1355573, 2024. 1
- [27] Daiki Miyake, Akihiro Iohara, Yu Saito, and Toshiyuki Tanaka. Negative-prompt inversion: Fast image inversion for editing with text-guided diffusion models. In *2025 IEEE/CVF Winter Conference on Applications of Computer Vision (WACV)*, pages 2063–2072. IEEE, 2025. 2, 3, 4, 8, 9

- [28] Ron Mokady, Amir Hertz, Kfir Aberman, Yael Pritch, and Daniel Cohen-Or. Null-text inversion for editing real images using guided diffusion models. In *Proceedings of the IEEE/CVF Conference on Computer Vision and Pattern Recognition*, pages 6038–6047, 2023. 2, 3, 4, 8, 9
- [29] Roy Or-El, Ron Kligler, Daniel Reichman, and Tal Hassner. Only a matter of style: Age transformation using a style-based regression model. In *ACM SIGGRAPH 2020 Conference Proceedings*, pages 1–12, 2020. 2
- [30] Luchao Qi, Jiaye Wu, Bang Gong, Annie N Wang, David W Jacobs, and Roni Sengupta. Mytimemachine: Personalized facial age transformation. *ACM Transactions on Graphics (TOG)*, 44(4):1–16, 2025. 3, 6, 7
- [31] Alec Radford, Jong Wook Kim, Chris Hallacy, Aditya Ramesh, Gabriel Goh, Sandhini Agarwal, Girish Sastry, Amanda Askell, Pamela Mishkin, Jack Clark, et al. Learning transferable visual models from natural language supervision. In *International conference on machine learning*, pages 8748–8763. PMLR, 2021. 3
- [32] Robin Rombach, Andreas Blattmann, Dominik Lorenz, Patrick Esser, and Björn Ommer. High-resolution image synthesis with latent diffusion models. In *Proceedings of the IEEE/CVF conference on computer vision and pattern recognition*, pages 10684–10695, 2022. 5
- [33] Rasmus Rothe, Radu Timofte, and Luc Van Gool. Dex: Deep expectation of apparent age from a single image. In *Proceedings of the IEEE international conference on computer vision workshops*, pages 10–15, 2015. 5
- [34] Jiaming Song, Chenlin Meng, and Stefano Ermon. Denoising diffusion implicit models. *arXiv preprint arXiv:2010.02502*, 2020. 4
- [35] Zepeng Su, Zhulin Liu, Zongyan Zhang, Tong Zhang, and CL Chen. Timebooth: Disentangled facial invariant representation for diverse and personalized face aging. In *Proceedings of the IEEE/CVF International Conference on Computer Vision*, pages 12147–12157, 2025. 3
- [36] Omer Tov, Yuval Alaluf, Yotam Nitzan, Or Patashnik, and Daniel Cohen-Or. Designing an encoder for stylegan image manipulation. *ACM Transactions on Graphics (TOG)*, 40(4): 1–14, 2021. 3
- [37] Narek Tumanyan, Michal Geyer, Shai Bagon, and Tali Dekel. Plug-and-play diffusion features for text-driven image-to-image translation. In *Proceedings of the IEEE/CVF Conference on Computer Vision and Pattern Recognition*, pages 1921–1930, 2023. 2, 3, 9, 12
- [38] Pavan Kumar Anasosalu Vasu, Fartash Faghri, Chun-Liang Li, Cem Koc, Nate True, Albert Antony, Gokula Santhanam, James Gabriel, Peter Grasch, Oncel Tuzel, et al. Fastvlm: Efficient vision encoding for vision language models. In *Proceedings of the Computer Vision and Pattern Recognition Conference*, pages 19769–19780, 2025. 3
- [39] Michael E Wall, Andreas Rechtsteiner, and Luis M Rocha. Singular value decomposition and principal component analysis. In *A practical approach to microarray data analysis*, pages 91–109. Springer, 2003. 2
- [40] Weiwei Wang, Weihong Deng, Jiani Hu, Junping Tao, and Yaohai Huang. Continuous face aging via self-estimated residual age embedding. In *Proceedings of the IEEE Conference on Computer Vision and Pattern Recognition (CVPR)*, pages 103–112, 2016. 3
- [41] Sihan Xu, Yidong Huang, Jiayi Pan, Ziqiao Ma, and Joyce Chai. Inversion-free image editing with natural language. *CoRR*, 2023. 3, 5
- [42] Hao Yang, Dun Huang, Bo Wang, Chunyan Sun, Baocai Yin, Rui Huang, Wei Liu, and Gang Yu. Face aging with identity-preserved conditional generative adversarial networks. In *Proceedings of the IEEE Conference on Computer Vision and Pattern Recognition (CVPR)*, pages 7939–7947, 2018. 3
- [43] Shiyu Yang, Jianqiang Zhang, Shiyu Lu, Ping Luo, Chao Chen, and Kui Jia. High-resolution face age editing. In *Proceedings of the IEEE/CVF Conference on Computer Vision and Pattern Recognition (CVPR)*, pages 11657–11666, 2021. 1, 2, 3, 5, 9
- [44] Shuang Zhang, Zhen Liu, Haibin Ling, and Chengming Gao. Lifespan age transformation synthesis. In *Proceedings of the IEEE International Conference on Computer Vision (ICCV)*, pages 903–911, 2017. 2, 5
- [45] Zhifei Zhang, Yang Song, and Hairong Qi. Age progression/regression by conditional adversarial autoencoder. In *Proceedings of the IEEE Conference on Computer Vision and Pattern Recognition (CVPR)*, pages 5810–5818, 2017. 3, 5
- [46] Gaspard Zoss, Prashanth Chandran, Eftychios Sifakis, Markus Gross, Paulo Gotardo, and Derek Bradley. Production-ready face re-aging for visual effects. *ACM Transactions on Graphics (TOG)*, 41(6):1–12, 2022. 1

👤 🔄 👤 **Face Time Traveller : Travel Through Ages Without Losing Identity**

Supplementary Material

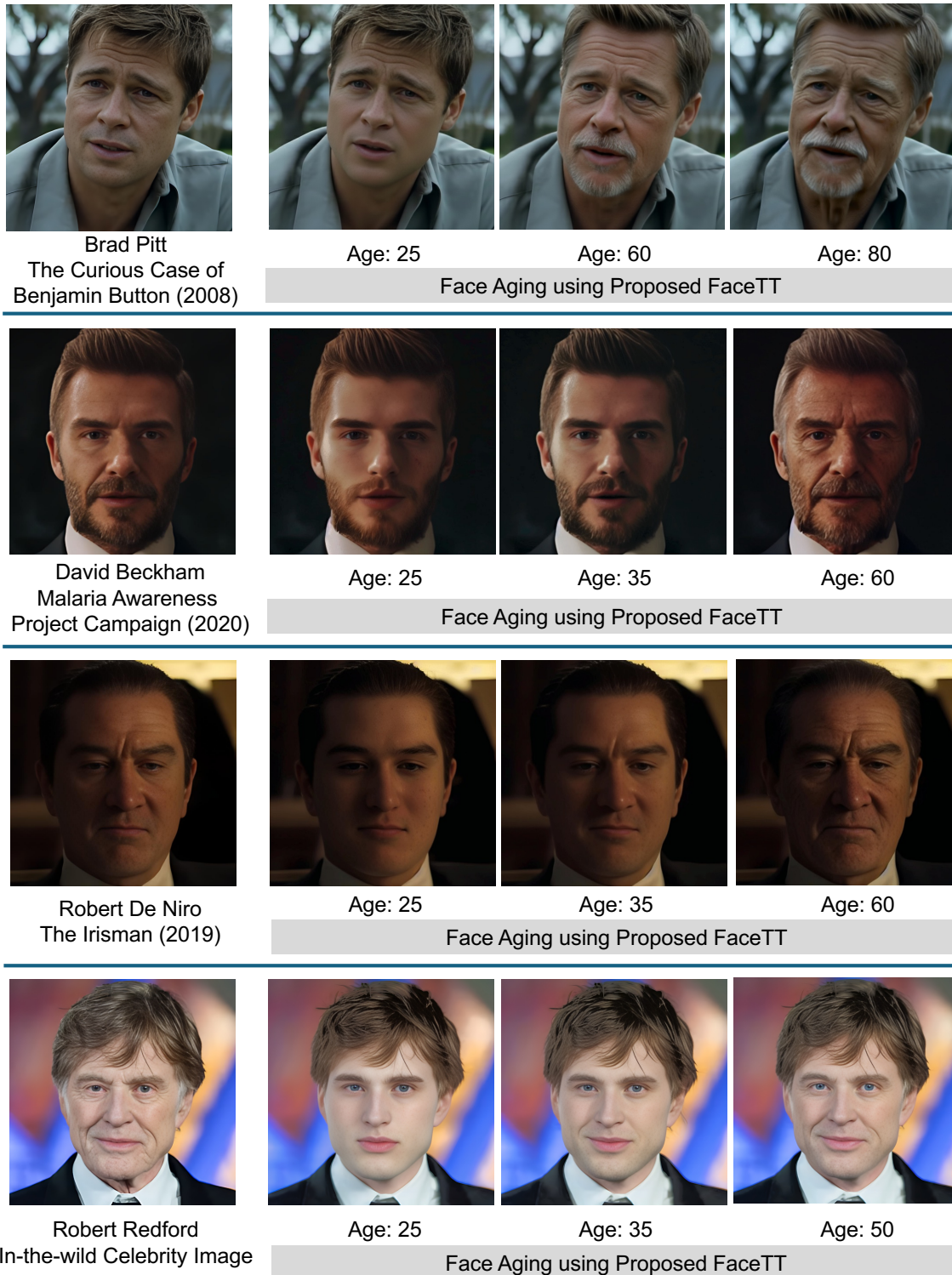


Figure S1. Results of our proposed method FaceTT in Film/Media application. FaceTT produces realistic and identity-preserving age progression on movie and in-the-wild celebrity images. These results demonstrate visually coherent transitions across young, middle-aged, and elderly appearances.

This supplementary presents below contents which we could not include in the main paper due to space constraints:

## Table of Contents

S1 Analysis on Cross- and Self-Attention ..... 2  
 S1.1 Probing Analysis ..... 2  
 S2 Additional Visual Comparison ..... 3  
 S3 Analysis on Identity Preservation ..... 3  
 S3.1 Cyclic / Reference based Aging Analysis ..... 3  
 S3.2 Short-Range Aging Analysis ..... 3  
 S4 Additional Ablation Analysis ..... 3  
 S4.1 Visual Analysis on Hyper-Parameters ..... 3  
 S4.2 Statistical Analysis on Hyper-Parameters ..... 7  
 S5 Analysis on Inversion & Editing Techniques ..... 8  
 S6 Ethical Concerns ..... 9  
 S7 Baseline Details ..... 9

### S1. Analysis on Cross- and Self-Attention

We investigate how cross-attention and self-attention in Stable Diffusion influence text-guided image editing through the U-Net model’s core components. Following the standard from [15], spatial features are linearly projected to form queries ( $Q$ ), while text features are transformed into keys ( $K$ ) and values ( $V$ ) for the cross-attention module. In the self-attention module,  $K$  and  $V$  are derived from spatial features. The attention mechanism is defined as:  $\text{Attention}(K, Q, V) = MV = \text{softmax}\left(\frac{QK^T}{\sqrt{d}}\right)V$ , where  $M_{i,j}$  represents the attention weights for aggregating the  $j$ -th token’s value at pixel  $i$ , with  $d$  being the dimensionality of  $K$  and  $Q$ .

Semantic modifications from natural language are categorized as rigid or non-rigid. Rigid changes, like background or visual element alterations, are handled using cross-attention [15], while non-rigid changes, such as adding/removing objects or changing actions, are managed with self-attention [23]. To evaluate whether the cross- and self-attention maps in face images contain meaningful semantic information, we employ a probing approach inspired by natural language processing (NLP) techniques [6, 24], as demonstrated in [23].

#### S1.1. Probing Analysis:

Following [23], we design and train a task-specific classifier consisting of a two-layer MLP to predict semantic categories from the attention maps. Using the prompt `Photo of a <2/10/30/50/70> years old <man/woman/boy/girl>`, we examine the effectiveness of the attention mechanisms. In this probing analysis, we avoid using our Face-Attribute-Aware refined prompts because they introduce additional semantic cues (e.g., skin texture, lifestyle conditions) that go beyond age and gender. Including these details would make the probe



Figure S2. Visualization of Cross- & Self-attention maps for age progression to 60-year-old appearance. Cross-attention maps highlight regions in the source image (e.g., eyes, nose, mouth) that align with target prompt `<Photo of a 60 years old woman/man>`. While self-attention visualization showcases top-7 components derived from singular value decomposition (SVD) [39], which is important to maintain identity and consistency.

Table S1. Probing accuracy of cross-attention maps w.r.t. different tokens. L denotes layers of the U-Net model.

Class	L-3	L-6	L-9	L-10	L-12	L-14	L-16	Avg.
Age 2	0.29	0.42	0.69	0.81	0.83	0.85	0.75	0.77
Age 10	0.60	0.20	0.70	0.92	0.90	0.90	0.63	0.69
Age 30	0.57	0.92	0.80	0.88	0.89	0.89	0.78	0.79
Age 50	0.50	0.87	0.80	0.72	0.87	0.87	0.41	0.81
Age 70	0.54	0.41	0.82	0.71	0.63	0.55	0.52	0.59
man	0.67	0.77	0.86	0.83	0.81	0.81	0.90	0.80
woman	0.62	0.80	0.83	0.78	0.76	0.82	0.84	0.78
boy	0.60	0.80	0.90	0.92	0.96	0.75	1.0	0.85
girl	0.50	0.70	0.92	0.84	0.87	0.70	0.90	0.78

rely on prompt semantics rather than the intrinsic information encoded in the attention maps. Using simple age-and-gender prompts ensures a controlled setting where we can directly evaluate what the model’s native attention layers capture without external influence.

**Cross-Attention Maps:** We explore the information captured by cross-attention maps by visualizing the attention patterns associated with each word in a prompt, as dis-

Table S2. Probing analysis of cross-attention maps w.r.t. difference tokens. The upper part shows the classification accuracy corresponding to the token `Photo`, and the lower shows results for `old`. L denotes layers of the U-Net model.

Class	L-3	L-6	L-9	L-10	L-12	L-14	L-16	Avg.
Age 2	0.85	0.78	0.89	0.80	0.93	0.85	0.91	0.87
Age 10	0.80	0.71	0.80	0.93	0.50	0.70	0.50	0.71
Age 30	0.76	0.85	0.86	0.90	0.75	0.96	0.71	0.83
Age 50	0.71	0.73	0.70	0.83	0.70	0.55	0.66	0.70
Age 70	0.61	0.67	0.62	0.70	0.66	0.50	0.60	0.62
Age 2	0.90	0.83	0.80	0.92	0.84	0.92	0.93	0.88
Age 10	0.85	0.90	0.87	0.80	1.0	0.75	0.70	0.84
Age 30	0.80	0.82	0.79	1.00	0.70	0.69	0.75	0.79
Age 50	0.83	0.80	0.70	0.79	0.63	0.62	0.61	0.71
Age 70	0.76	0.71	0.59	0.83	0.52	0.70	0.58	0.67

Table S3. Probing accuracy of self-attention maps w.r.t. different tokens. L denotes layers of the U-Net model.

Class	L-3	L-6	L-9	L-10	L-12	L-14	L-16	Avg.
Age 2	0.00	0.00	0.00	0.20	0.00	0.00	0.00	0.028
Age 10	0.18	0.06	0.70	0.35	0.80	0.25	0.90	0.46
Age 30	0.00	0.00	0.00	0.00	0.5	1.0	0.00	0.21
Age 50	0.00	0.1	0.00	0.00	0.66	0.23	0.10	0.16
Age 70	0.00	0.00	0.82	0.05	0.25	0.00	0.23	0.19
man	0.36	0.68	0.45	0.90	0.80	0.30	0.60	0.58
woman	0.33	0.41	0.83	0.58	0.63	0.10	0.81	0.53
boy	0.30	0.21	0.80	0.87	0.91	0.65	0.80	0.76
girl	0.47	0.10	0.00	0.69	0.70	0.41	0.00	0.34

played in Figure S2. Each map highlights areas related to specific words, indicating that cross-attention retains rigid semantic details. In the context of the facial re-aging task, these rigid details include wrinkles and changes in skin texture, variations in the fullness of the cheeks and lips, as well as the development of age-related marks such as fine lines or sagging skin. Table S1 presents the classification performance of our trained classifier, demonstrating high accuracy, especially for the age and person categories.

We also investigate whether cross-attention maps associated with non-edited words contain rigid information. This analysis is essential because text embeddings generated by transformer-based encoders [20, 31] preserve the contextual details of sentences. By using prompts like `Photo of a <age> years old <person>`, our experiments (shown in Table S2) reveal that both the tokens `Photo` and `old` exhibit significantly high classification accuracy. This finding indicates that both tokens carry rigid semantic information related to faces.

**Self-Attention Maps:** In contrast, self-attention maps exhibit different behaviors and are analyzed similarly. Table S3 shows that the classifier struggles to recognize categories (age and person) accurately, indicating that self-attention maps encode non-rigid information, or structural rather than categorical details. For our task, this structural information includes the relative positions of the eyes, nose, mouth, and the overall shape of the face (e.g., jawline). Fig-

ure S2 illustrates that self-attention maps preserve the original structure of the image.

This shows that cross-attention maps encode semantic features for category identification, while self-attention maps preserve structural integrity for image coherence.

## S2. Additional Visual Comparisons

This section offers a visual comparison between our FaceTT and the state-of-the-art (SOTA) methods i.e., HRFAE [43], CUSP [11], and FADING [5]. From Figure S3 to S5, one can observe that HRFAE preserves identity but struggles with exaggerated features. CUSP provides smooth transitions; however, it comes at the cost of losing fine details in extreme aging. FADING generates plausible results but often produces overly smooth textures or inconsistencies. In contrast, our method maintains identity and delivers highly realistic aging effects across diverse facial structures and expressions.

## S3. Analysis on Identity Preservation

### S3.1. Cyclic / Reference based Aging Analysis:

We conducted Cyclic and Reference-based Identity Similarity evaluation on a five-celebrity in-the-wild age-progression test set. Results for one celebrity (Tom Cruise) are shown in the main paper (Figure 2), while the remaining four—Brad Pitt, Leonardo DiCaprio, Matt Damon, and Robert Downey Jr.—are presented in Figure S6. Across all age cycles, our method consistently yields higher identity similarity than HRFAE, CUSP, and FADING, demonstrating stronger face aging with identity preservation in both forward and reverse age transformations.

### S3.2. Short-Range Aging Analysis

To further assess the identity-preservation capability of our method, we perform a Short-Range Aging Analysis that evaluates identity stability under fine-grained age perturbations. Figure 9 in the main paper shows examples for two identities, demonstrating consistent identity retention across closely spaced target ages. Additional results for two more identities are provided in Figure S7, further highlighting the robustness of our approach in maintaining facial structure and appearance under small age variations.

## S4. Additional Ablation Analysis

### S4.1. Visual Analysis on Hyper-Parameters

Figure S8 analyzes the impact of the hyper-parameter  $\xi$  used in *Angular Inversion*. Low  $\xi$  values (specifically,  $\xi = 0.1, 0.5$ ) result in minimal changes, allowing the input identity to be preserved but producing weaker re-aging effects. Conversely, high  $\xi$  values (such as  $\xi = 2.0$ ) lead to

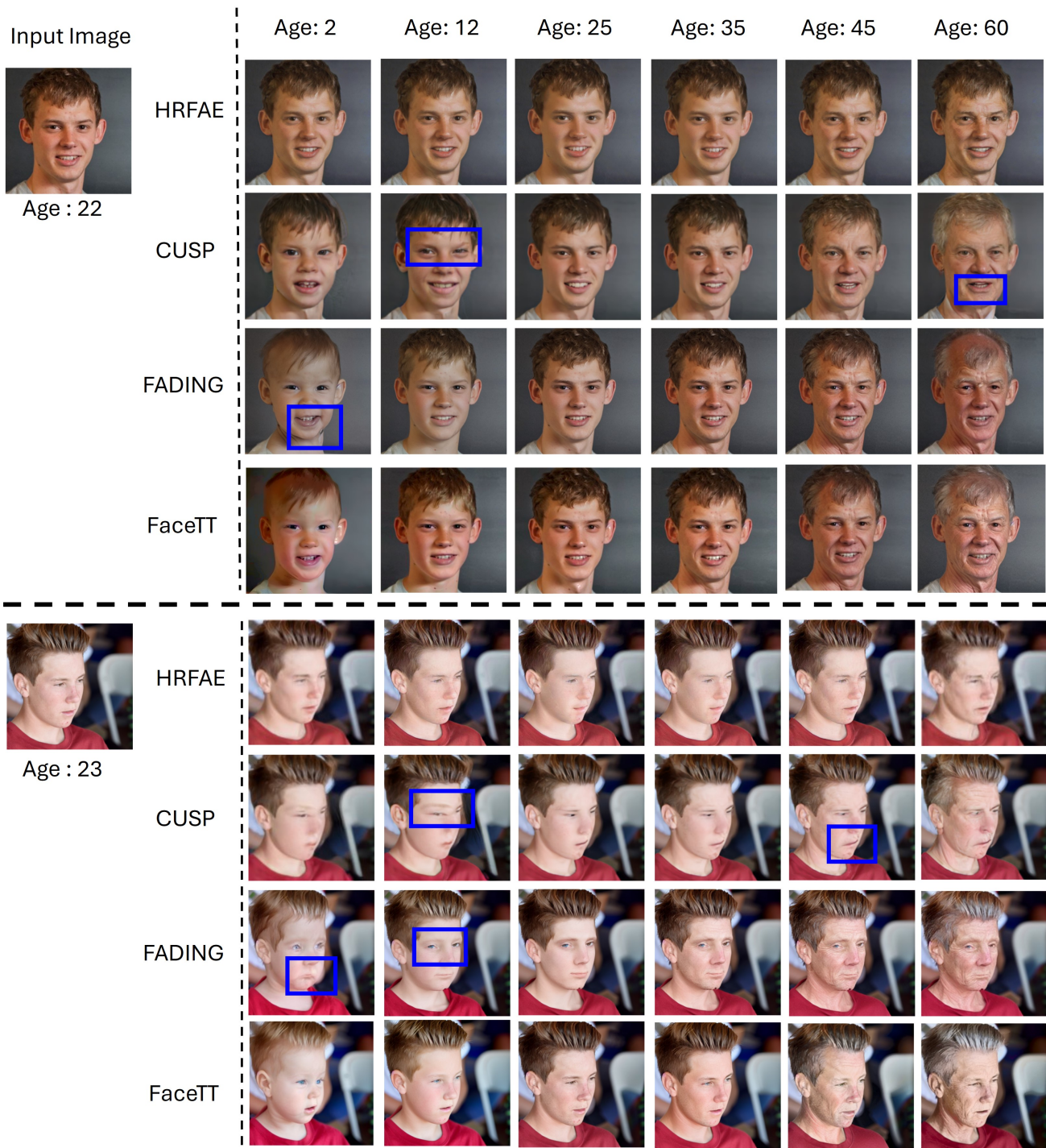


Figure S3. Comparison of facial re-aging across different age targets using HRFAE, CUSP, FADING, and our FaceTT method (Part 1). Across both examples, FaceTT produces the most consistent identity preservation and the most realistic aging trajectories from early childhood (Age: 2) to older adulthood (Age: 60). Competing methods exhibit notable artifacts: HRFAE often fails to introduce meaningful age changes and tends to output visually similar faces across age ranges; CUSP frequently produces structural distortions and texture inconsistencies (blue boxes), especially in the eyes and mouth regions; and FADING, while capable of stronger aging effects, suffers from identity drift and unnatural facial modifications (blue boxes). In contrast, FaceTT generates smooth, coherent age transitions with preserved facial geometry and identity cues, while accurately reflecting age-specific features such as fuller cheeks in youth, subtle mid-life changes, and realistic wrinkle patterns at older ages.

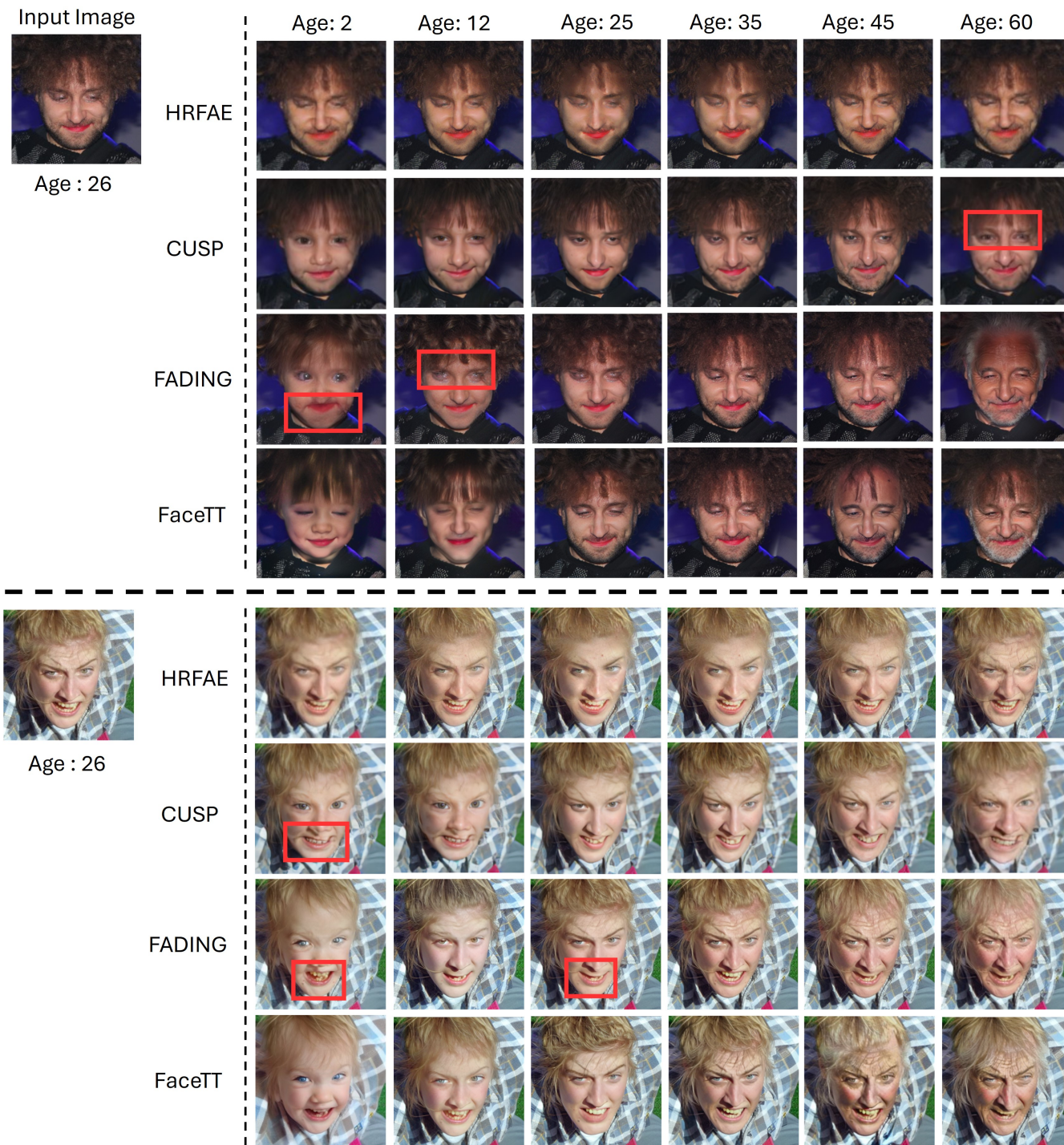


Figure S4. Additional visual comparison of facial re-aging methods. (Part 2, continued from Figure S3)

excessive alterations, causing distortions and a loss of identity. The optimal balance is found at  $\xi = 1.2$ , which provides realistic re-aging while maintaining identity, as shown in the first and third rows. This highlights  $\xi = 1.2$  as the preferred choice for high-quality results.

Figure S9 examines the effect of  $\eta_{th}$  in *Adaptive Attention Control*, which determines the transition between self-attention and cross-attention adaptation. When  $\eta_{th}$  is too low (e.g., 0.03), the attention mechanism primarily preserves source characteristics, leading to insufficient aging

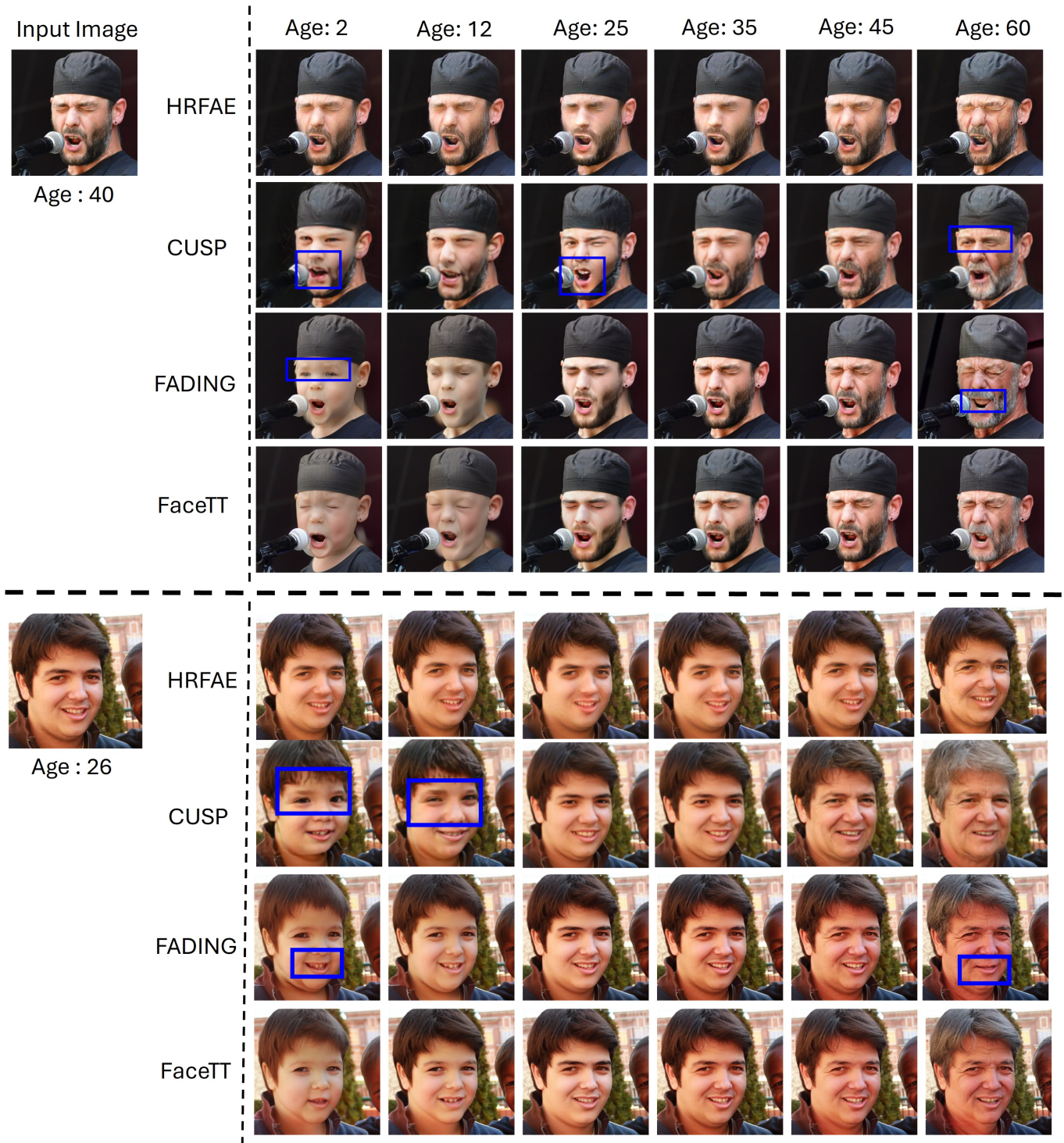


Figure S5. Additional visual comparison of facial re-aging methods. (Part 3, continued from Figure S3)

effects. Conversely, setting  $\eta_{th}$  too high (e.g., 0.06) results in excessive modification of details, introducing artifacts. The best balance occurs at  $\eta_{th} = 0.05$ , enabling natural aging transformations while maintaining identity consistency.

Figure S10 evaluates the impact of  $(\tau_1, \tau_2)$ , which regu-

lates the selection of either cross-attention or self-attention or mixture of both (based on the value of  $\eta_{th}$ ) in *Adaptive Attention Control*. Low  $\tau_1$  values (e.g., 25) retain too many source attributes, preventing effective aging transformations. On the other hand, high values (e.g., 40) lead to

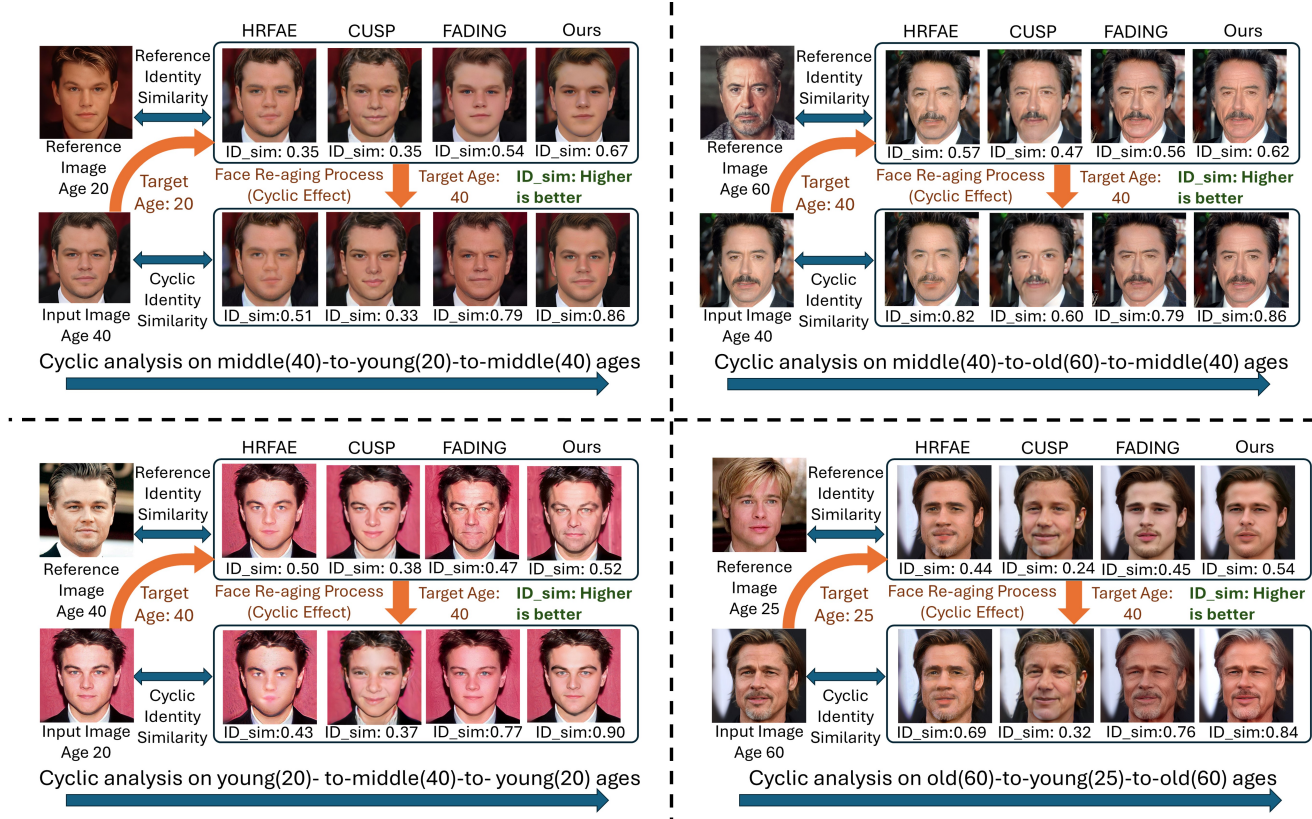


Figure S6. Cyclic Identity Similarity protocol for evaluating identity preservation across age transitions. For each input celebrity image, we perform age progression and regression cycles (e.g., 40→20→40 (top left), 40→60→40 (top right), 20→40→20 (bottom left), 60→25→60 (bottom right)) and compute both Reference Identity Similarity (between the re-aged output and a real image at the target age) and Cyclic Identity Similarity (between the input and its cyclic reconstruction). Across all age cycles, our method consistently achieves higher identity similarity compared to HRFAE, CUSP, and FADING, demonstrating more faithful identity retention during both forward and reverse age transformations.

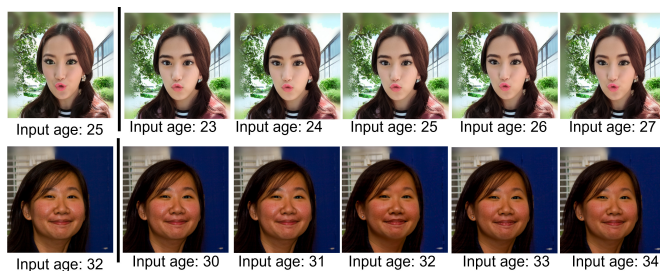


Figure S7. Short-range aging analysis for identity preservation. Each row shows aging results within a narrow age window ( $\pm 2$  years) around the input age. Our method preserves identity exceptionally well across all nearby target ages, producing nearly indistinguishable facial structure, expression, and texture from the original input. This demonstrates that even under fine-grained age perturbations—where inconsistencies are easiest to detect—FaceTT maintains stable and coherent identity features without drifting or introducing artifacts.

exaggerated changes, distorting facial features. Similarly, improper selection of  $\tau_2$  affects the smoothness of the transformation. The optimal configuration,  $(\tau_1, \tau_2) = (35, 15)$ , provides the best trade-off between structural consistency and realistic aging effects, as demonstrated in Figure S10.

#### S4.2. Statistical Analysis of Hyper-Parameter

To further validate our approach, we incorporated a statistical analysis in Fig. S11, where the mean  $\pm$  standard deviation of the predicted ages is reported for different age groups across various hyperparameter configurations. This evaluation was conducted on the CelebA-HQ dataset to assess the consistency and accuracy of the generated age transformations. The statistical trends observed support the robustness of our chosen hyperparameters, ensuring realistic and demographically appropriate age progression across the dataset.

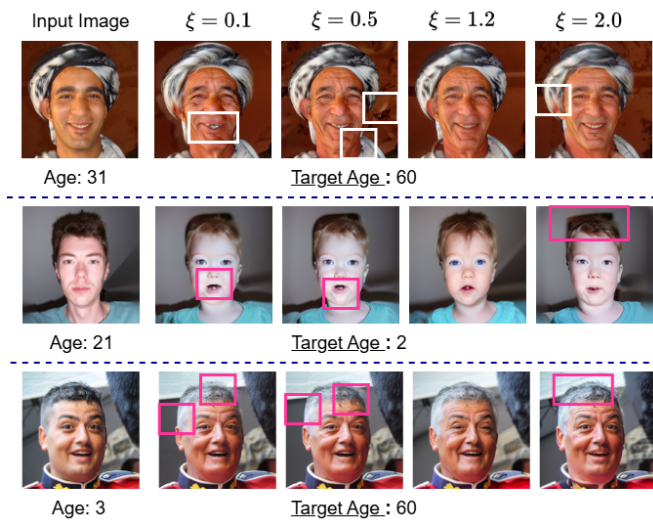


Figure S8. Ablation analysis on different  $\xi$  values being used in the proposed *Angular Inversion* technique. The results demonstrate how different  $\xi$  values influence the balance between preserving identity and achieving accurate transformations to match the target prompts (e.g., age 2 or 60 years). Among the tested values,  $\xi = 1.2$  provides the best results, striking an optimal trade-off between transformation fidelity and identity preservation.

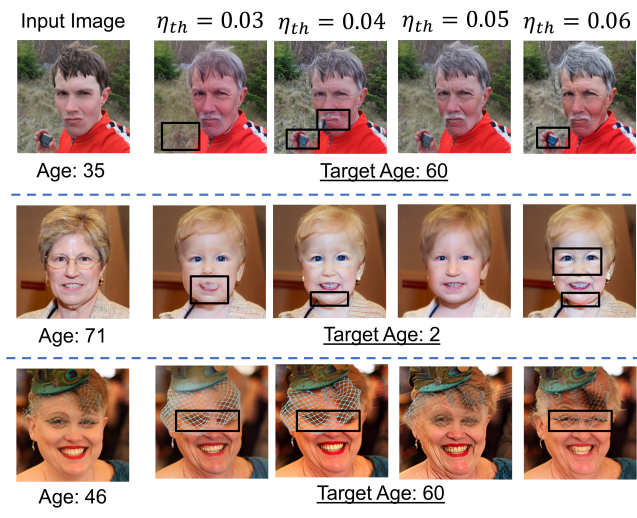


Figure S9. Ablation analysis on different  $\eta_{th}$  values in the proposed *Adaptive Attention Control* technique. The results illustrate how varying  $\eta_{th}$  impacts the trade-off between maintaining structural consistency and achieving accurate aging transformations. Lower values (e.g.,  $\eta_{th} = 0.03$ ) retain excessive source attributes, leading to incomplete aging effects, while higher values (e.g.,  $\eta_{th} = 0.06$ ) introduce artifacts and distortions in fine details (highlighted in black boxes). The optimal value,  $\eta_{th} = 0.05$ , provides the best balance, ensuring realistic aging transformations while preserving important identity and contextual details.

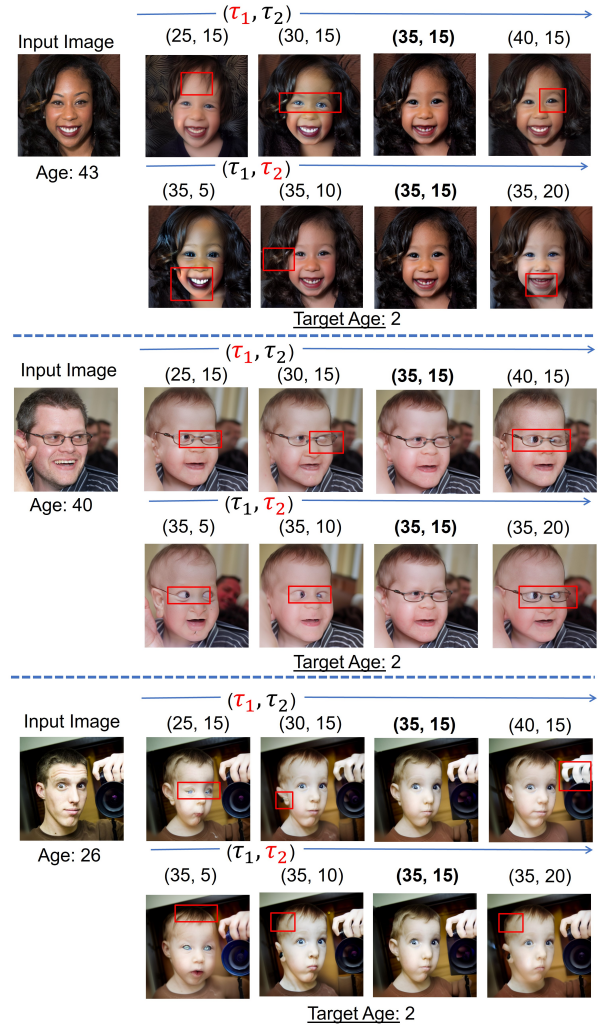


Figure S10. Ablation analysis on different  $(\tau_1, \tau_2)$  values in the *Adaptive Attention Control* technique, investigating their effect on balancing structural preservation and non-rigid transformations. Lower values of  $\tau_1$  (e.g., 25) retain more source characteristics but limit the effectiveness of the transformation, while higher values (e.g., 40) can lead to excessive modifications, causing distortions in fine details (highlighted in red boxes). Similarly, an improper choice of  $\tau_2$  can result in either overly rigid transformations or undesirable warping effects. The best balance is achieved with  $(\tau_1, \tau_2) = (35, 15)$ , ensuring natural age transformation while preserving key identity features.

### S5. Analysis on Inversion & Editing Techniques

The additional analysis is illustrated in Figures S12, which shows a visual comparison between the proposed *Angular Inversion* and existing inversion techniques [14, 18, 27, 28]. This comparison shows that the Proximal Inversion [14] achieves partial alignment with target prompts but struggles with fine details, resulting in inconsistent transformations. While Negative-Prompt Inversion [27] enhances

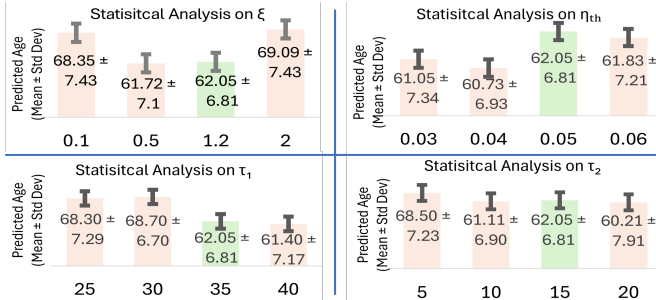


Figure S11. Statistical analysis. Targeted predicted age:  $65.14 \pm 4.86$

Table S4. Comparative analysis on CelebA-HQ dataset for young-to-60 task. Best score: in red, second-best score: in green.

Techniques	Predicted age	Blur ↓	Gender ↑	Smiling ↑	Neutral ↑	Happy ↑
Analysis on Inversion techniques						
Real Images	$65.14 \pm 4.86$	1.73	—	—	—	—
Null-Text [28]	$69.88 \pm 6.20$	2.18	98.44	76.17	56.54	73.19
Negative [27]	$69.35 \pm 5.51$	2.69	98.23	74.35	61.77	69.19
Proximal [14]	$68.39 \pm 6.74$	2.49	98.13	73.99	63.94	71.98
Direct [18]	$61.84 \pm 6.80$	2.18	99.71	73.74	64.65	66.23
Angular (Proposed)	$62.05 \pm 6.81$	2.18	99.79	78.31	62.67	72.17
Analysis on editing techniques						
Real Images	$65.14 \pm 4.86$	1.73	—	—	—	—
P2P [15]	$57.31 \pm 4.23$	2.31	97.40	72.07	61.19	65.77
MasaCtrl [4]	$57.23 \pm 7.65$	2.57	96.90	75.39	64.25	66.32
PnP [37]	$69.35 \pm 6.26$	2.30	98.67	78.22	62.15	69.85
FPE [23]	$68.45 \pm 6.32$	2.27	97.53	73.39	62.36	67.20
AAC (Proposed)	$62.05 \pm 6.81$	2.18	99.79	78.31	62.67	72.17

alignment, it introduces distortions, particularly in extreme age changes. Null-Text inversion [28] provides better prompt alignment but compromises identity and realism, leading to overly smoothed features. Direct Inversion [18] maintains facial structure but lacks the adaptability needed for extreme transformations, which results in artifacts. In contrast, our *Angular Inversion* method captures fine details and preserves semantic alignment and identity, resulting in realistic and coherent age transformations. Its balanced performance proves its superiority over existing methods.

Figures S13 show an additional comparison of the proposed AAC with existing image editing techniques, including P2P [15], PnP [37], MasaCtrl [4], and FPE [23]. It shows that P2P struggles to balance alignment and identity, often resulting in exaggerated or distorted features. While PnP is more consistent, it is still prone to artifacts, especially in extreme cases. MasaCtrl improves prompt fidelity but tends to overemphasize features, resulting in unnatural transformations. FPE balances structure and identity but lacks adaptability in extreme cases, resulting in overly smooth results. In contrast, our AAC outperforms these methods by modulating attention mechanisms to achieve semantic fidelity and identity preservation. It delivers realistic transformations, handling challenging cases like extreme age regression or progression with natural, coherent outputs.

## S6. Ethical Concerns

The development of facial re-aging technology raises several ethical considerations that must be addressed to ensure responsible usage. The ability to manipulate facial features across different age groups brings up concerns about privacy, identity misuse, and potential exploitation. For example, re-aging technology could be misused to create deceptive content, such as deepfakes, which might lead to misinformation or harm an individual’s reputation. This challenge is applied to all image editing methods in general. However, advancements in detecting and mitigating malicious edits are evolving quickly. We believe our work will support these efforts by providing insights and access of the proposed image editing and generation process.

## S7. Baseline Details

Our proposed framework for facial re-aging is compared with three SOTA methods [5, 11, 43]. Details of these baselines are as follows:

- **HRFAE** [43], a hybrid model that uses feature-aligned encoders to preserve identity and achieve photorealistic re-aging effects. However, HRFAE often struggles with extreme age transformations, leading to minor inconsistencies in older age predictions.
  - **CUSP** [11] combines cycle-consistent adversarial networks with spatial priors to achieve smooth age progression and regression. Despite its ability, CUSP sometimes fails to capture fine-grained aging details accurately.
  - **FADING** [5] uses null-text inversion [28] and attention control for facial image editing with a pre-trained diffusion model. Despite high-quality results, it faces challenges with identity consistency in extreme age edits and is computationally intensive for real-time applications.
- To validate the effectiveness of our proposed *angular inversion* technique, we compare it with existing inversion techniques [14, 18, 27, 28].
- **Null-Text Inversion** [28] uses pivot tuning with null-text prompts for better alignment but suffers from inefficiencies in computation.
  - **Negative-Prompt Inversion** [27] speeds up inversion by approximating DDIM inversion, but sacrifices reconstruction quality.
  - **Proximal Inversion** [14] improves Negative-Prompt Inversion by using proximal guidance, but struggles with latent space disruptions, particularly for complex transformations.
  - **Direct Inversion** [18] separates source and target branches for better content preservation but faces challenges with complex edits, especially when large attribute shifts are required.

We also validate the proposed AAC editing technique with existing baselines [4, 15, 23, 37].



Figure S12. Comparison of different inversion methods for facial re-aging across multiple target ages (2 → 60 years). Proximal, Null-Text, Direct, and DDPM inversion each introduce distortions or identity drift during the re-aging process. Proximal Inversion often produces inconsistent geometry and blurry structural changes, leading to unnatural aging transitions. Null-Text Inversion exhibits significant shape warping and texture artifacts (blue boxes), particularly in early-age predictions. Direct Inversion suffers from identity inconsistency and incorrect facial proportions across ages, while DDPM Inversion frequently alters key identity features (blue boxes), causing the re-aged outputs to deviate from the input subject. In contrast, *Angular Inversion* yields stable, high-fidelity reconstructions with smooth and realistic age progression, maintaining consistent identity cues from childhood to old age. The results highlight that *Angular Inversion* achieves the most reliable and artifact-free initialization for age editing, enabling accurate transformations across the entire age spectrum.

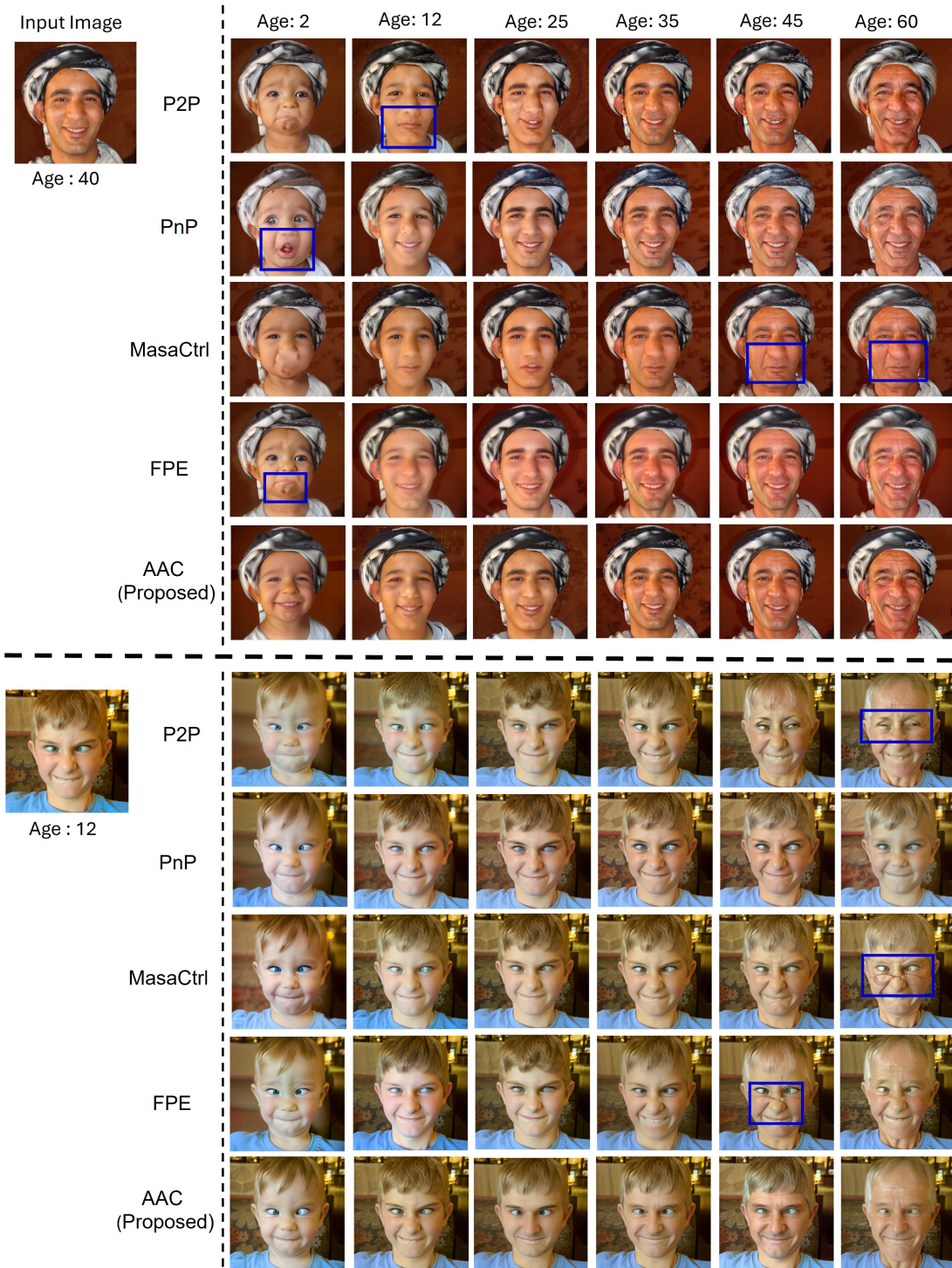


Figure S13. Comparison of age editing using P2P, PnP, MasaCtrl, FPE, and our *Adaptive Attention Control (AAC)* across target ages 2→60. Existing attention-based editing methods exhibit noticeable artifacts and identity inconsistencies: P2P often produces over-smoothed faces and distorted geometry (blue boxes), especially for younger ages; PnP struggles with preserving identity and frequently introduces incorrect mouth and eye structures; MasaCtrl shows unstable attention modulation, leading to drifted identity and inconsistent aging patterns; and FPE tends to hallucinate textures or distort facial regions (blue boxes), particularly in older targets. In contrast, AAC achieves smooth and coherent age progression while consistently preserving identity, facial structure, and attribute integrity across the entire age spectrum. The results demonstrate that Adaptive Attention Control provides more precise, stable, and semantically aligned guidance than prior attention-editing approaches.

- **Prompt-to-Prompt (P2P)** [15] adjusts cross-attention to maintain spatial consistency in edits. Although effective in many scenarios, it struggles with transformations requiring significant structural changes.
- **Plug-and-Play (PnP)** [37] modifies attention maps for text-driven image editing but introduces minor artifacts.
- **MasaCtrl** [4] enables mutual self-attention control but generates noticeable artifacts in challenging transformations.
- **FPE** [23] modifies self-attention maps for stable edits but struggles with precise age-specific effects.